

Universidade de Lisboa

Faculdade de Ciências

Departamento de Física



# **Novel Approaches to Cardiac Magnetic Resonance Postprocessing:**

**Pressure gradients across aortic coarctation and flow kinetic  
energy within the ventricles**

**João Filipe Cardoso Pires Timóteo Fernandes**

Dissertação

Mestrado Integrado em Engenharia Biomédica e Biofísica

Perfil de Sinais e Imagens Médicas

2013



Universidade de Lisboa

Faculdade de Ciências

Departamento de Física



# **Novel Approaches to Cardiac Magnetic Resonance Postprocessing:**

**Pressure gradients across aortic coarctation and flow kinetic energy within the ventricles**

**João Filipe Cardoso Pires Timóteo Fernandes**

Dissertação

Mestrado Integrado em Engenharia Biomédica e Biofísica

Perfil de Sinais e Imagens Médicas

Supervisor FCUL: Prof. Rita Nunes

Orientador DHZB: Prof. Dr. Titus Kühne

2013

*"I find that the harder I work, the more luck I seem to have."*

- Thomas Jefferson (1743-1826)

# Abstract

*The blood flow physiology is one of the less understood cardiovascular areas, due to limited resources available in the past. Nowadays, new cardiovascular imaging techniques, such as 4D phases contrast (PC-MRI) Cardiovascular Magnetic Resonance (CMR) are emerging, increasing the quality of flow visualization and quantification.*

*Two of the less explored quantification parameters are the basis of this Master thesis project: Pressure differences across an aortic stenosis and visualization and quantification of the blood flow kinetic energy (KE) within the moving ventricles. To achieve this goal two postprocessing softwares were refined and applied.*

*To study the pressure gradient across an aortic stenosis, thirteen patients were scanned CMR prior to catheterization. Relative pressure fields were computed from PC-MRI by solving the Pressure Poisson equation. Vessel pressure field map was obtained from each voxel differences to a defined reference location with known absolute pressure (from catheterization and from non-invasive arm pressure measurements). The agreement between these techniques was determined at five measurement sites along the aorta.*

*To calculate and visualize the KE per time step an algorithm combined the PC-MRI flow data with a moving ventricle mask. Then the ventricle KE was plotted over the cardiac cycle. The KE was calculated within left ventricles (LV) with mitral regurgitation (MR), right ventricles (RV) with pulmonary regurgitation (PR) and healthy LV and RV. The respective curves and maps were compared. The kinetic energy study presents here the first results of a future larger project.*

*The pressure gradient study results show that in a clinical setting of aortic coarctation, pressure fields can accurately be computed from PC-MRI. The KE study shows that, in regurgitations cases, KE tends to be higher than in healthy ventricles.*

*This multi study project exemplifies how the use post-processing techniques can maximise the amount of information obtained non-invasively from the CMR.*

**Key Words: Blood flow, four-dimensional phase contrast MRI, Pressure Gradient, Kinetic Energy**

## Resumo

*A forma como o sangue flui dentro do corpo humano tem sido desde há muito tempo um assunto de interesse para a comunidade médico-científica. No entanto, devido aos recursos limitados é também um dos aspectos fisiológicos menos entendidos ao nível cardiovascular. Na actualidade, a introdução de novas técnicas de imagiologia, como a ultra-sonografia de Doppler ou a ressonância magnética de contraste de fase em tempo real (4D PC-MRI), tem permitido uma evolução significativa na aquisição, traduzida num muito maior nível de detalhe na sua visualização e quantificação. Esta evolução é suportada por um crescente número de investigações com maior profundidade ao nível do fluxo sanguíneo. Actualmente, com o cálculo da Angiografia Cardiovascular por Ressonância Magnética (PC-MRA) calculado a partir da imagem de PC-MRI adquirida, já é possível medir o fluxo do sangue e velocidade com resultados muito aceitáveis.*

*No entanto, ainda existem alguns parâmetros menos explorados ao nível do fluxo sanguíneo. Dois destes parâmetros formam a base desta dissertação de mestrado: o cálculo do gradiente de pressão no caso de uma estenose na artéria aorta; a visualização e quantificação da energia cinética, ao longo do ciclo cardíaco, do fluxo sanguíneo no interior de ventrículos saudáveis e com patologias. Dado que estes parâmetros ainda não estão muito estudados e que para a obtenção destas medidas é necessário o uso programas de processamento de imagens de ressonância magnética cardiovascular (CMR), o primeiro grande objectivo deste projecto foi estabelecer colaborações com programadores destes programas e ajudar a aperfeiçoá-los. Tal passo tinha por objectivo a familiarização e principalmente o desenvolvimento dos programas por forma a ser possível executar as medições pretendidas, identificando e solucionando problemas devidos a processos físicos relacionados com a aquisição, erros de implementação do programa ou no tratamento das imagens. Após os programas serem melhorados, prosseguiu-se para os objectivos principais deste projecto.*

*O estudo do gradiente de pressão através de uma estenose na aorta apresentava como aliciante o facto de comparar esta técnica totalmente não invasiva com a técnica que é prática corrente em ambiente clínico: o cateterismo cardíaco, técnica invasiva de diagnóstico e tratamento. Ora, está estabelecido que apenas se efectua a colocação de um stent (através de cateterização) numa estenose aórtica quando o gradiente de pressão através da estenose é superior a 20mmHg. Assim sendo, muitas vezes é usada a cateterização apenas com fim de diagnosticar, pois nem sempre o gradiente é superior ao requerido clinicamente para indicação de cirurgia. Assim sendo este estudo tem como objectivo comparar os valores de pressão obtidos de forma invasiva, com os calculados com base nas imagens PC-MRA, resolvendo a equação de pressão de Poisson.*

*Treze pacientes (na faixa etária de 13 a 52 anos,  $n = 7$  masculino,  $n = 6$  do sexo feminino) com estenose na aorta foram estudados por CMR antes de se submeterem a um cateterismo cardíaco. Campos de pressão relativos foram calculados a partir da imagem de PC-MRI. Um campo de pressão absoluta ao longo de toda a aorta segmentada foi obtido pela adição da pressão relativa de cada voxel a um valor absoluto conhecido numa região predefinida da aorta. O valor absoluto foi obtido quer por cateterização (pressões dinâmicas) quer por métodos CMR baseados em medições de pressão no braço direito (pressões estáticas) equivalentes às da aorta ascendente. Seguidamente foram comparados as pressões resultantes destes dois métodos*

*em cinco locais de medição ao longo da aorta. Para melhor interpretação dos resultados foi feita uma análise estatística.*

*Em todos os 5 locais de medição estudados, os coeficientes de correlação entre as medidas variaram entre 0,86 e 0,97. O Teste de Bland-Altman demonstrou boa concordância entre os gradientes de pressão de pico sistólica através da coarctação. As diferenças entre os métodos não foram significativas ( $p > 0,2$ ). Assim sendo, pode-se concluir com este estudo que em situações clínicas, campos de pressão podem ser calculados de forma precisa a partir de velocidades de fluxo derivados 4D- VEC - MRI. Esta técnica não-invasiva pode assim evoluir para uma alternativa ao diagnóstico com recurso à cateterização invasiva.*

*Uma vez que num estudo anterior (Carlsson et al.) foi estudada a evolução da energia cinética no interior de ventrículos saudáveis ao longo de um ciclo cardíaco, este estudo tem como objectivo primário desenvolver um procedimento cujos resultados sejam coerentes com os de Carlsson et al.. Em seguida, pretende também oferecer uma primeira comparação visual e quantitativa entre as energias cinéticas ventriculares de voluntários saudáveis versus pacientes com regurgitação numa válvula cardíaca (válvula mitral no caso de se considerar o ventrículo esquerdo antes e após intervenção, e válvula pulmonar no caso de se considerar o ventrículo direito antes de intervenção).*

*A segmentação 3D semiautomática do lúmen ventricular foi feita para cada intervalo temporal do ciclo cardíaco. Desta resultou uma máscara do respectivo ventrículo em movimento durante um ciclo cardíaco. Simultaneamente foi calculado o PC-MRA contendo a informação das velocidades do fluxo sanguíneo. Para calcular e visualizar a energia cinética per cada intervalo temporal foi desenvolvido um módulo num software de programação cujo algoritmo combina os dados de fluxo de PC-RM com uma máscara de ventrículo em movimento. Foram então comparados os gráficos e figuras obtidos entre ventrículos saudáveis e ventrículos com regurgitação valvular (quer para o ventrículo direito quer para o ventrículo esquerdo).*

*Estes são os primeiros resultados obtidos pelo estudo da energia cinética ventricular, dado que este projecto ainda se encontra em desenvolvimento. Ainda assim pode-se comprovar que os resultados obtidos segundo esta metodologia são coerentes com os obtidos por Carlsson et al. (ao nível dos ventrículos saudáveis). Pode-se também comprovar que ventrículos com maior volume são mais propensos a apresentar relativamente maior energia cinética. Observou-se também que a energia cinética tende a ser mais elevada em locais em que existe mais turbulência e caminhos de fluxo de sangue não lineares como as válvulas cardíacas.*

*Em conclusão, estas técnicas emergentes de análise de imagens cardiovasculares potenciam uma melhor compreensão do sistema cardiovascular. No futuro poderão permitir um melhor diagnóstico assim como um planeamento terapêutico personalizado de patologias cardiovasculares. Isto iria aumentar a taxa de sucesso e, por conseguinte, reduzir a principal causa patológica de mortes entre a população humana.*

*De notar ainda que o estudo dos gradientes de pressão através da aorta resultou já num artigo que aguarda neste momento aprovação.*

**Palavras-chave: fluxo sanguíneo, Ressonância magnética de contraste de fase, Gradiente de Pressão, Energia Cinética**

# Acknowledgements

Firstly I would like to thank my parents for meeting and getting along with each other, and for giving life and education in every sense of both words to two amazing boys, specially the second one, Tiago, with who I learn to share almost everything, from ultimate challenges to a fantastic country full of smiles and special characters like Panduca, both Poohs, Dumbeca and Ibérico.

Next I would like to congratulate my 4 grandparents for connecting themselves and valorize so much the wealthy life they have. They are really an example of strength to me.

After causing so much scary moments to them, it is very important to me, to feel the faith and the believe that my godparents as well as my full (31 member) family have on me.

I have also to apologize to Gancho, Hugo, Íris and all my friends for the “not that often” lack of communication. There is a big thanks you to be given also to Ji Yiyi, Tiago Silva and João Periquito for surviving in the same house as me during 9 months. And also a special thanks for speechless support of Dworaczyk family during the weekends.

Next, I would like to refer the importance of Prof. Eduardo Ducla Soares, Prof. Alexandre Andrade, Prof. Pedro Cavaleiro Miranda and all the Institute of Biofisics and Biomedical Engineering (IBEB) team (Prof. Pedro Almeida, Prof. Hugo Ferreira, Prof. Nuno Matela, Prof. Pedro Salvador e Prof. Rita Nunes) for building up such a reference course with a complete works plan that allows the students to learn, practice, develop self-working methods and have 2 internships that, at my view, are fundamental for introducing students to the real work developed on Biomedical field.

A very special thanks to Prof. Rita Nunes, who besides accepting to be my coordinator, was very patient and supportive to me and to my work.

But none of this Master thesis would be possible if it was not the receptivity and vision of Prof. Dr. Titus Kühne. His friendly Boss approach always questioning my methods was from outmost importance to the evolution of the work as well was my own evolution within research area. Actually, all the Deutsche Herzzentrum Berlin (DHZB) MRT team was very welcome and ready to hear my problems and help me, and therefore I am now in big debt to Dr. Nadya Al-Wakeel, Alireza Khasheei, Dr. Davide Santoro, Dr. Eugene Riesenkauff, Dr. Dhafer Al Qahtani and Lili, and to them and their families I wish everything good. Also big thanks are due to those who collaborated with our team, the MevisFlow and CAIPI teams and Leonid Goubergrits.

Note also the founding importance of ERASMUS internship projects, DHZB and specially my family for the financial support.

At last, but most importantly I would like to say “dziękuję bardzo” to Karolina, for being sited next to me while I am writing my master thesis dissertation and mainly for offering me the best thing one can offer: LOVE!



# Contents

<b>ABSTRACT</b>	<b>5</b>
<b>RESUMO</b>	<b>6</b>
<b>ACKNOWLEDGEMENTS</b>	<b>8</b>
<b>CONTENTS</b>	<b>9</b>
<b>ACRONYM LIST</b>	<b>11</b>
<b>FIGURE LIST</b>	<b>12</b>
<b>TABLE LIST</b>	<b>15</b>
<b>MOTIVATION</b>	<b>16</b>
<b>THESIS OUTLINE</b>	<b>17</b>
<b>1 GENERAL CONCEPTS</b>	<b>18</b>
1.1 ANATOMY AND PHYSIOLOGY	18
1.1.1 <i>Heart</i>	18
1.1.2 <i>Aorta</i>	19
1.2 BLOOD FLOW DIAGNOSIS AND QUANTIFICATION	20
1.2.1 <i>Cardiac Catheterization</i>	20
1.2.2 <i>Angiography</i>	22
1.2.3 <i>CT</i>	22
1.2.4 <i>PET</i>	22
1.2.5 <i>Echocardiography</i>	23
1.2.6 <i>Hybrid imaging</i>	24
1.3 CARDIOVASCULAR MAGNETIC RESONANCE IMAGING	25
1.3.1 <i>Acquisition</i>	28
1.3.2 <i>Pre-processing and PC-MRA calculation</i>	29
1.3.3 <i>Data analysis</i>	29
1.4 BLOOD FLOW IMAGING STATE OF THE ART	30
<b>2 OBJECTIVES</b>	<b>32</b>
2.1 SOFTWARE REFINEMENT	32
2.2 PRESSURE GRADIENT ACROSS AN AORTIC COARCTATION	32
2.3 KINETIC ENERGY WITHIN THE VENTRICLES	33
2.4 OTHER OBJECTIVES	33
<b>3 WORK'S PLANNING</b>	<b>34</b>
3.1 COLLABORATIONS	35
<b>4 MATERIAL</b>	<b>37</b>

4.1	CMR SCANNER	37
4.2	POSTPROCESSING SOFTWARES	38
4.2.1	<i>MevisFlow</i>	38
4.2.2	<i>CAIPI</i>	42
4.2.3	<i>MevisLab</i>	43
<b>5</b>	<b>PRESSURE GRADIENT ACROSS AN COA STUDY</b>	<b>44</b>
5.1	METHODOLOGY	44
5.1.1	<i>Statistical analysis</i>	47
5.2	RESULTS	49
5.3	DISCUSSION	52
5.3.1	<i>Limitations</i>	55
<b>6</b>	<b>KINETIC ENERGY WITHIN THE VENTRICLES STUDY</b>	<b>56</b>
6.1	METHODOLOGY	56
6.2	RESULTS	59
6.3	DISCUSSION	65
<b>7</b>	<b>CONCLUSION</b>	<b>69</b>
<b>8</b>	<b>BIBLIOGRAPHY</b>	<b>70</b>

## Acronym List

2D .....	two-dimensional
3CHle.....	3 chambers view left anatomical image
3CHri.....	3 chambers view right anatomical image
3D .....	three-dimensional
4D .....	four-dimensional
BSA .....	Body Surface Area
CoA .....	Coarctation of the aorta
CMR.....	Cardiovascular Magnetic Resonance
CT.....	Computed tomography
CTA.....	Computed tomographic angiography
CVD.....	Cardiovascular Diseases
CVI.....	Cardiovascular Imaging
EDV.....	end-Diastolic Volume
EF .....	Ejection Fraction
ESV .....	end-Systolic Volume
FOV .....	Field of View
HR .....	Heart Rate
KE.....	Kinetic Energy
LV.....	Left Ventricle
MR.....	Mitral Regurgitation
MIP.....	Maximum Intensity Projection images
MRI .....	Magnetic Resonance Imaging
PC-MRA.....	Phase Contrast Magnetic Resonance Angiography
PC-MRI.....	Phase Contrast Magnetic Resonance Imaging
PR .....	Pulmonary Regurgitation
ROI.....	Region of Interest
RV .....	Right Ventricle
RVOT.....	Right Ventricle Outflow Tract view plane
SAX.....	Short Axis view plane
SNR .....	Signal-to-noise ratio
SV .....	Stroke Volume
TRA-BFFE .....	Balanced fast field echo

# Figure List

<i>Figure 1.1 Frontal heart diagram with anatomy major landmarks and venous (blue) and arterial (red) blood flow directions through the atria, ventricles, and associated vessels.[3]</i>	18
<i>Figure 1.2 Heart ventricles cross-sectional view diagrams showing the dilated (ventricular diastole) and contracted (systolic) ventricle myocardium.[3]</i>	19
<i>Figure 1.3 Schematic frontal view of aorta artery within the human body divided in the 4 major portions: ascending thoracic aorta, aortic arch, descending thoracic aorta and abdominal aorta. In the figure are also present the associated arteries.[2]</i>	19
<i>Figure 1.4 A: Catheterization of the right side hearth cavities or pulmonary artery. The catheter is inserted into the femoral vein and advanced through the inferior vena cava, or, in antecubital or basilic vein, through the superior vena cava. B: Catheterization of the left side hearth cavities or aortic artery. The catheter is inserted into the femoral artery or the antecubital artery and advanced through the aortic different portions.[4]</i>	21
<i>Figure 1.5 Colour Doppler echocardiogram in parasternal long axis view showing mitral regurgitation (MR jet), the heart cavities: left ventricle (LV), left atrium (LA), right ventricle (RV) and aorta artery (Ao).[1]</i>	23
<i>Figure 1.6 A: Data acquisition for 3D cine velocity acquisition using navigator gating for respiration control. The navigator gating control is placed above the lung and establishes a gating window for image acquisition. Therefore not all the heart beats are considered when acquiring PC-MRI images. B: Schematic illustration of ECG-gated three-directional phase-contrast MR (3D-PC) sequence used to measure blood flow. Velocity encoding was performed using four modules: a reference module and one for each of the 3 different velocity directions Vx, Vy and Vz) per time frame, also known as time step, (1 time frame establishes the PC-MRI time resolution). X, Y, and Z are the three (slice-select, phase-encode, and frequency-encode) gradient axes used. C: Raw data per slice and per time frame obtained from the four velocity vector extraction (One Magnitude image and different velocity components Vx, Vy and Vz velocity images). In this image it is possible to verify that stationary protons appear grey (orange arrow), flow in one direction appears white (yellow arrow), and flow in the opposite direction appears black (red arrow)[6]</i>	26
<i>Figure 1.7 Image processing for obtaining a 3D PC-MRA of a healthy thoracic aorta. A PC-MRA image is obtained by calculating (voxel by voxel) the absolute velocity resulting from the combination of the 3 different acquired velocity components, with image masking based on the magnitude image. A: RAW data acquired from a PC-MRI with magnitude provided as reference and the 3 different velocity components Vx, Vy and Vz). B: The resulting PC-MRA images can be displayed as a maximum intensity projection (MIP) or as a semi-transparent 3D iso-surface which can be combined with 3D flow visualization.[6]</i>	28
<i>Figure 4.1 Pre-Processing menu, that allows a 4D phase-offset error correction to be made using third-order polynomials (Eddy current correction) as well as a phase unwrapping (still under development). The PC-MRA is also calculated here.</i>	38
<i>Figure 4.2 Flow analysis menu, where it is possible to draw and select the ROIs, visualize and export vector fields (A), tracking particle flow or pathlines (B), visualise the connectivity map, compute and visualize the blood flow pressure, and see and export the temporal evolution of the vessel cross-sectional Area, velocity, blood flow and pressure for a single cardiac cycle.</i>	39

Figure 4.3 Vessel segmentation menu where it is possible to segment semi-automatically (based on markers and filters) several cardiovascular structures for the same image set. ....	39
Figure 4.4 After the application of the phase unwrapping algorithm, the phase wrap had not been fully corrected. ....	40
Figure 4.5 An ROI should always be kept in the same plane in which it was drawn. In this and some other cases the contour becomes 3dimensional and as a consequence it is impossible to have information (see graphic above) for a 2D contour in the time steps. ....	40
Figure 4.6 The particles emitted went outside the segmented vessel, which can happen because of a bad image acquisition or a bug in the software. ....	41
Figure 4.7 When region coloration is used for the pathlines, the colour of the pathlines should be the same as the ROI from which they are originated. In this and some other cases the streamline is either all green or has different colours (similar to what would be obtained if the ID coloration had been used for the pathlines). ....	41
Figure 4.8 Moving ventricle masks of healthy volunteers obtained with the CAIPI segmentation tool. A: LV mask of end-diastole (highest blood volume) time step B: LV mask of end-systole (lowest blood volume) time step. The A and B masks were obtained from the same patient and exemplify the moving LV masks set; C: RV mask of end-diastole (highest blood volume) time step D: RV mask of end-systole (lowest blood volume) time step. The C and D masks were obtained from the same patient and exemplify the moving RV masks set. All the masks sets have 25 different masks correspondent to the 25 time steps over a cardiac cycle. ....	42
Figure 4.9 Example of valve planes clip on a healthy LV segmentation. The 2 valve planes determined by the user (yellow regions) correspond to the mitral valve (1) and to the aortic valve (2). A: Short axis view of the LV basis, where it is possible to visualize both chosen clip planes. B: Longitudinal view of the LV, where is also possible to visualize the valve clip planes chosen. ....	43
Figure 5.1 A: MR angiography of the aorta in one representative patient. The six locations for pressure measurements are shown. B to F: CMR derived 4D colour coded pressure fields calibrated with catheter, from beginning of systole to end-diastole (B: early systole, C: peak systole, D: early diastole, E: mid diastole, F: end diastole). The shown data belong to a 46 year old female patient with re-coarctation. The peak-systolic pressure gradient across the stenosis was 19 mmHg measured by catheter and 21 mmHg measured by CMR. ....	45
Figure 5.2 Pressure profiles of the ascending and descending aorta measured by catheterization and by CMR pressure field method with catheter calibration. The pressure profiles were obtained from a 13 year old female patient with re-coarctation in the aortic arch. The pressure profiles of the ascending aorta and the descending aorta were measured in position 2 and 6 as indicated in Figure 1, panel A. Note the timing difference in peak-systolic pressures between ascending and descending aorta (arrows) ....	47
Figure 5.3 Bland-Altman plot for end-diastolic pressures measured by catheterization and CMR pressure fields in n=13 patients at different measurement locations in the ascending and descending aorta. ....	50
Figure 5.4 Bland-Altman plot for peak-systolic pressures measured by catheterization and CMR pressure fields in n=13 patients at different measurement locations in the ascending and descending aorta. ....	50
Figure 5.5 Bland-Altman plot for peak-systolic pressure gradients measured by catheterization and CMR pressure fields between two different locations in the ascending and descending aorta (location 1 and 6, Figure 1, panel A). Calibration was done with dynamic pressures obtained from catheterization (see methods section for details). ....	51

Figure 5.6 Bland-Altman plot for peak-systolic pressure gradient measured by catheterization and CMR pressure fields between two different locations in the ascending and descending aorta (location 1 and 6, Figure 1, panel A). Calibration was done with static pressures (see methods section for details)..... 51

Figure 6.1 (A) MevisLab module for KE visualization and calculation. This module was developed in this project and is divided in 3 minor steps: The first (1) consists on applying the segmented mask to the PC-MRA image in the respective time step. In the second (2) the number of voxel within the mask is calculated as well as the total volume of the mask. In the third step (3) the KE is calculated voxel by voxel together with the total KE per time step. The module outputs are the 2D colour gradient KE image (B) and the total KE and blood flow volume (C) of the masked cardiovascular structure..... 58

Figure 6.2 A: Blood flow kinetic energy (KE) curves (in mJ) over the cardiac cycle (time normalized) within a healthy subject left ventricle (LV) obtained by Carlsson et al. in a 1.5 and a 3 Tesla CMR scanners.[5] All the remaining curves (B to D) compare a healthy subject and a patient with mitral insufficiency before and after an intervention to the respective valve. B: KE curves (in mJ) over the cardiac cycle (time normalized); C: Volume curves (in mL) over the cardiac cycle (time normalized); D: Volume normalized KE curves over the cardiac cycle (time normalized). These are the first results obtained from the presented methodology applied to LV. These are also the first ever results considering KE within a diseased LV. .... 59

Figure 6.3 Peak left ventricle (LV) systole (moment in which more blood is being ejected from the ventricle) images of 3D blood flow tracing with velocity colour scale (up) and 2D kinetic energy (KE) colour gradient in the long axis longitudinal view (down). The blood flow tracing images include a static segmentation of the LV, left atrium (LA) and aorta artery (Ao), whereas the KE include only the LV. The images on the left (A and D) were obtained from a healthy subject. The middle images (B and E) were obtained from a patient with mitral valve insufficiency before intervention. The images on the right (C and F) were also from the same patient, but after intervention. (AL: left-anterior direction according the anatomical position, HR: right-head direction according to the anatomical position of descending aorta)..... 60

Figure 6.4 Peak left ventricle (LV) diastole (moment in which less blood is being ejected from the ventricle) images of 3D blood flow tracing with velocity colour scale (up) and 2D kinetic energy (KE) colour gradient in the long axis longitudinal view (down). The blood flow tracing images include a static segmentation of the LV, left atrium (LA) and aorta artery (Ao), whereas the KE include only the LV. The left images (A and D) were obtained from a healthy subject. The middle images (B and E) were obtained from a patient with mitral valve insufficiency before intervention. The right images (C and F) were also from the same patient, but after intervention. (AL: left-anterior direction according the anatomical position, HR: right-head direction according the anatomical position descending aorta) ..... 61

Figure 6.5 Peak right ventricle (RV) systole (moment in which more blood is being ejected from the ventricle) images of 3D blood flow tracing with velocity colour scale (up) and 2D kinetic energy (KE) colour gradient in the long axis longitudinal view (down). The blood flow tracing images include a static segmentation of the RV, right atrium (RA) and pulmonary artery (PA), whereas the KE include only the RV. The left images (A and C) were obtained from a healthy subject. The right images (B and D) were obtained from a patient with pulmonary valve insufficiency before intervention. (An: anterior direction according to the anatomical position, H: head direction according to the anatomical position descending aorta)..... 62

Figure 6.6 Peak right ventricle (RV) diastole (moment in which more blood is entering in the ventricle) images of 3D blood flow tracing with velocity colour scale (up) and 2D kinetic energy (KE) colour gradient in

the long axis longitudinal view (down). The blood flow tracing images include a static segmentation of the RV, right atrium (RA) and pulmonary artery (PA), whereas the KE include only the RV. The left images (A and C) were obtained from a healthy subject. The right images (B and D) were obtained from a patient with pulmonary valve insufficiency before intervention. (An: anterior direction according to the anatomical position, H: head direction according to the anatomical position descending aorta)..... 63

Figure 6.7 A: Blood flow kinetic energy (KE) curves (in mJ) over the cardiac cycle (time normalized) within a healthy subject right ventricle (RV) obtained by Carlsson et al. in a 1.5 and a 3 Tesla CMR scanner. (Carlsson et al). All the remaining curves (B to D) compare a healthy subject and a patient with pulmonary insufficiency before intervention to the respective valve. B: KE curves (in mJ) over the cardiac cycle (time normalized); C: Volume curves (in mL) over the cardiac cycle (time normalized); D: Volume normalized KE curves over the cardiac cycle (time normalized). These are the first results obtained from the presented methodology applied to RV. These are also the first ever results considering KE within a diseased RV. .... 64

## Table List

Table 3.1 Work plan of the project by expectable dates and tasks. ....	35
Table 5.1 Patient characteristics and pressure gradients, * Blood pressure was measured on the right upper arm with the Riva-Rocchi (RR) method, † Gradients were measured between peak-systolic pressure values at locations 2 and 6 (Figure 5.1A), (CoA: Coarctation; Re-CoA: Re-Coarctation) .....	49

# Motivation

Nowadays cardiovascular diseases are the most death causing diseases in the world, killing more than 17 million of people per year.[7] These are concerning numbers that justify the importance of studying and understanding every single detail of the cardiovascular function as well as its relation with external factors that can potentially lead to Cardiovascular Diseases (CVD). Actually this is the reason why so many grants are given and so many studies are performed worldwide about the heart, vessels and cardiovascular pathologies. This is also why there are researchers from as different backgrounds as Medicine, Biomedical Engineering, Informatics, Mathematics among others, working together to minimize this big global issue.

This work presents two studies that demonstrate new techniques or measurements such as the non-invasive calculation of the aortic pressure gradient across a coarctation and the measurement of blood flow kinetic energy (KE) with the ventricles.

The first study tries to offer an alternative for diagnostic catheterization. The pressure gradient clinically accepted in order to proceed to a stent placement intervention with catheter when the aortic coarctation is 20mmHg.[8, 9] So, many times an aortic coarctation is detected and diagnosed invasively by catheterization, but when the gradient is lower than 20mmHg no intervention is made. This means that an invasive procedure is conducted, with the inherent risks of infection, further cardiovascular issues and in a few cases even death.[10] The approach presented here aims to introduce a totally non-invasive diagnosis procedure based on CMR imaging as alternative to diagnosis by catheter.

There is relatively little knowledge concerning the blood flow behaviour inside a ventricle since it is very difficult to trace, predict or even measure the blood flow inside the biggest and constantly moving cavities of the cardiovascular system(the ventricles).[11] Therefore the second study included in this dissertation introduces a new measurement of ventricular function: blood flow KE. This measurement aims to provide a better understanding of the blood flow behaviour within healthy and non-healthy ventricles, and it is possible that in the future it may be included in CMR imaging exams to help diagnosing heart diseases for a and potentially help plan personalized treatments.



# Thesis Outline

This dissertation is structured in 7 main chapters.

Chapter 1 presents the general concepts, introducing the anatomy and physiology of the heart and aorta artery, respectively the organ and vessel of the cardiovascular system that will be the basis of these dissertation studies. Following this section, a summary of the presently available techniques that can be used for blood flow analysis will be presented: Cardiac Catheterization, Angiography, Computer tomography (CT), Positron emission tomography (PET), Echocardiography and Hybrid imaging and finally cardiovascular magnetic resonance (CMR). CMR is presented in its own subchapter since it is the imaging technique that is the basis of this project. In the CMR subchapter, the basic concepts of image acquisition, pre-processing and data analysis are presented. Finally the current state of the art of blood flow imaging will be presented.

In Chapter 2 the objectives of this master thesis project are presented. Due to the new approaches used, the first objective was to make a refinement of the softwares used to obtain the intended measurements. The objectives of both studies (Pressure gradient across an aortic stenosis and KE within the ventricles) are then presented. The last subchapter of the objectives chapter presents a list of other small objectives also aimed by this work.

In Chapter 3 a table is presented detailing the project planning with the developed tasks and respective dates. In this chapter the collaborations established during the project development are also mentioned.

In Chapter 4 a small presentation of the material used during the project research is made. Firstly the characteristics of the CMR scanner used are presented. Secondly a small description of the postprocessing softwares (MevisFlow, CAIPI and MevisLab all developed by MeVis Medical Solutions AG and Fraunhofer MEVIS in Bremen, Germany) is presented, including the main tools that were used.

In Chapter 5 the “Pressure gradient across an aortic coarctation” study is presented, divided in methodology, results and discussion.

In Chapter 6 the “Kinetic energy within the ventricles” study is described. In the methodology section of the kinetic energy study the procedure used to visualize and obtain a curve of the flow within a patient’s ventricle during a single heartbeat is presented. Here only the first results and a preliminary interpretation will be presented as this study is still under development.

In Chapter 7, a final overview of the present master thesis project will be presented including conclusions regarding future perspectives of postprocessing of CMR imaging.

# 1 General Concepts

## 1.1 Anatomy and physiology

### 1.1.1 Heart

The heart is the main organ of the circulatory system, since it is the one that pumps the blood through the whole organism, and thus providing all body cells with oxygen and nutrients. The Heart is a muscular organ with an approximately conical form located in the middle of the chest between the lungs.[12]

In healthy individuals the blood has to pass through the heart twice per each cardiac cycle. Anatomically, the heart is divided in two sides (left and right) and each side has two cavities: the atrium, a thin-walled and relatively small cavity where the blood enters the heart, and the ventricle, a cavity bigger and thicker than the atrium, and located just below it. The right side of the heart is responsible for transporting blood poor in oxygen and rich in carbon dioxide (CO<sub>2</sub>) from the body to the lungs (where gas exchanges that allow the

increase in O<sub>2</sub> concentration and decrease in the CO<sub>2</sub> concentration occur). The left side of the heart is responsible for receiving the already oxygenated blood and pumping it into the other parts of the body (Figure 1.1). The one-way flow of blood through the heart chambers on both sides of the heart valves is managed by the tricuspid and bicuspid semilunar valves. Note also that each time the heart beats (in an average adult) about 80mL of blood is expelled.[13]

Since the function of the atria collects blood and conveys it to ventricles in the same way on both sides, there is no big structural difference between them apart from the number of veins leading to them. The ventricles are, however, very different given the very significant structural differences. Since the lungs are close to the heart, the pulmonary blood vessels are relatively short and there is not that much ventricular work needed to pump the blood through the whole

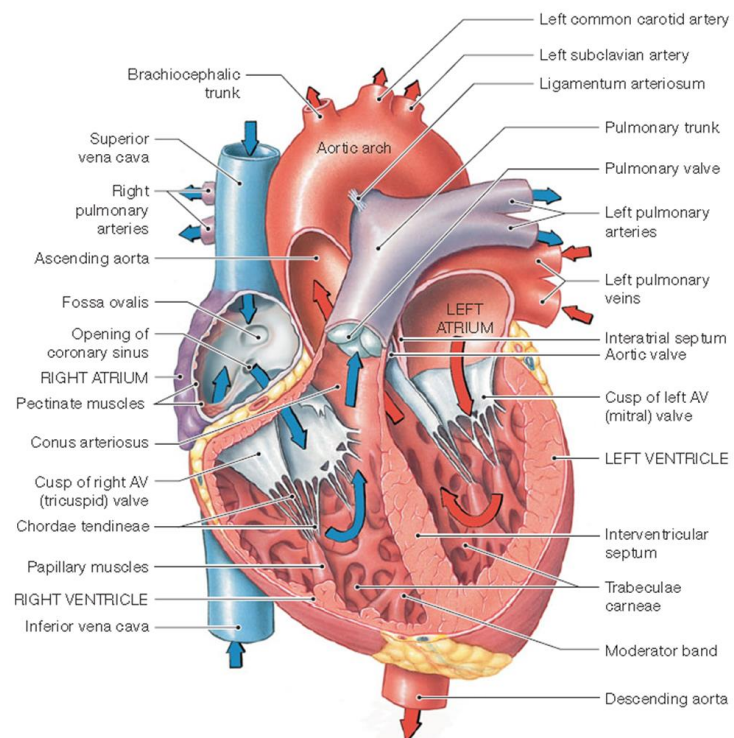


Figure 1.1 Frontal heart diagram with anatomy major landmarks and venous (blue) and arterial (red) blood flow directions through the atria, ventricles, and associated vessels.[3]

body. It is therefore natural that the LV has an extremely thick muscular wall and is round in cross section whereas the RV have a thinner muscular wall (see Figure 1.2).[3]

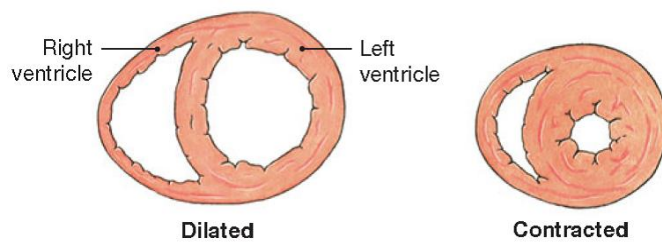


Figure 1.2 Heart ventricles cross-sectional view diagrams showing the dilated (ventricular diastole) and contracted (systolic) ventricle myocardium.[3]

The anatomy of the wall also influences the contraction of the ventricles. Most RV contraction occurs along its long axis from base to apex, particularly in the outer wall (free wall), with a smaller component from radial contraction of LV. This is in contrast to the systolic emptying of the LV, which involves significant radial contraction. This makes the blood flow differently in LV than in RV concerning paths, velocities or pressures within the ventricles.[11]

### 1.1.2 Aorta

The aorta is an elastic artery that carries the stroke volume of blood that goes out of the LV in each heart beat and for that, a healthy aorta can have diameters up to 2.5 cm (see Figure 1.3). Since it contains a high density of elastic fibers, and relatively few smooth muscle cells the aorta can tolerate the pressure changes characteristic of the cardiac cycle. During LV systole, pressures rise rapidly and aorta expands. When the pressure drops in LV diastole, the elastic fibers recoil to their original dimensions. Their recoil slows the pressure drops in the adjacent

smaller vessels during LV diastole. Therefore, aorta helps to make blood flow. This function is important since the blood pressure has a direct effect on the blood flow behaviour: The greater the pressure oscillations, the greater

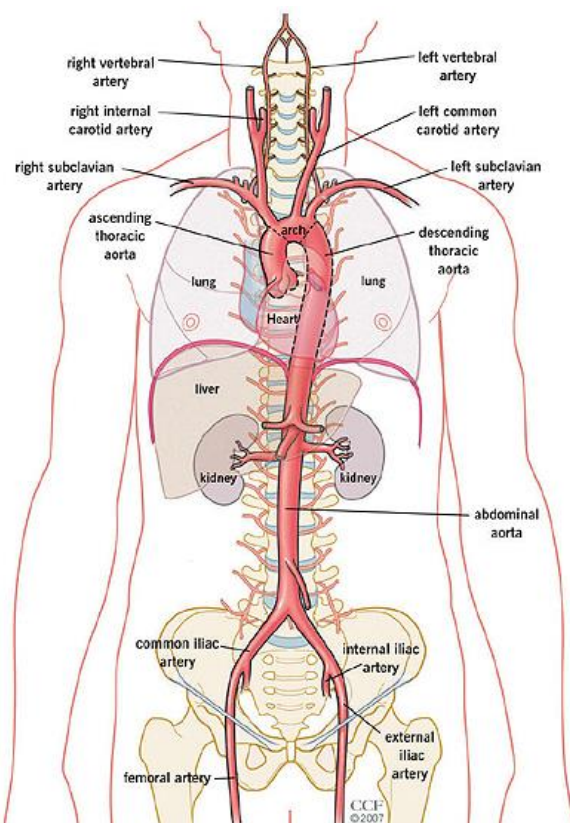


Figure 1.3 Schematic frontal view of aorta artery within the human body divided in the 4 major portions: ascending thoracic aorta, aortic arch, descending thoracic aorta and abdominal aorta. In the figure are also present the associated arteries.[2]

the changes in blood flow. As a consequence, the wall characteristics of the elastic arteries are the main reason for the absence of pressure oscillations when the blood reaches the arterioles in healthy subjects.

Therefore, an aorta with some condition can raise significant cardiovascular issues. One of the most common diseases in the aorta is the Coarctation of the aorta (CoA) accounting for 5-8% of all congenital heart defects.[8] Surgical or interventional treatment of CoA is associated with low morbidity. However, Re-CoA occurs frequently and is often associated with persistent arterial hypertension and shows increased morbidity at long-term.[14]

Current treatment strategies are focussing on the elimination of pressure gradients across the site of CoA. According to clinical guidelines intervention is recommended, amongst others, at a systolic gradient of  $> 20$  mmHg measured by catheterization in children[15] or, in adults, by catheterization or non-invasively.[8, 9]

## **1.2 Blood flow Diagnosis and Quantification**

Both Cardiac catheterization and Cardiovascular Imaging (CVI) enclose panoply of modalities which can be chosen according to exam time, health-risk factors, price of the exam, and, essentially, the objective of the study or diagnosis. A complete description of all these modalities would need an extended report, and so here only a brief introduction is made covering their basic concepts as well as their applicability to evaluate or not blood flow and pressure.

### **1.2.1 Cardiac Catheterization**

Cardiac catheterization is mainly a diagnostic technique which does a comprehensive intravascular examination of the function of the heart. One or more catheters are inserted into the cardiovascular system through a peripheral blood vessel either in the arm (antecubital artery or vein) or leg (femoral artery or vein) under x-ray guidance (Figure 1.4). The catheterization can be used to measure several blood functional and structural parameters as blood pressures [16], cardiac output [17] or myocardial metabolism [18] as well as be used as intravascular CVI as catheter angiography [19, 20], intravascular ultrasonography.[21]

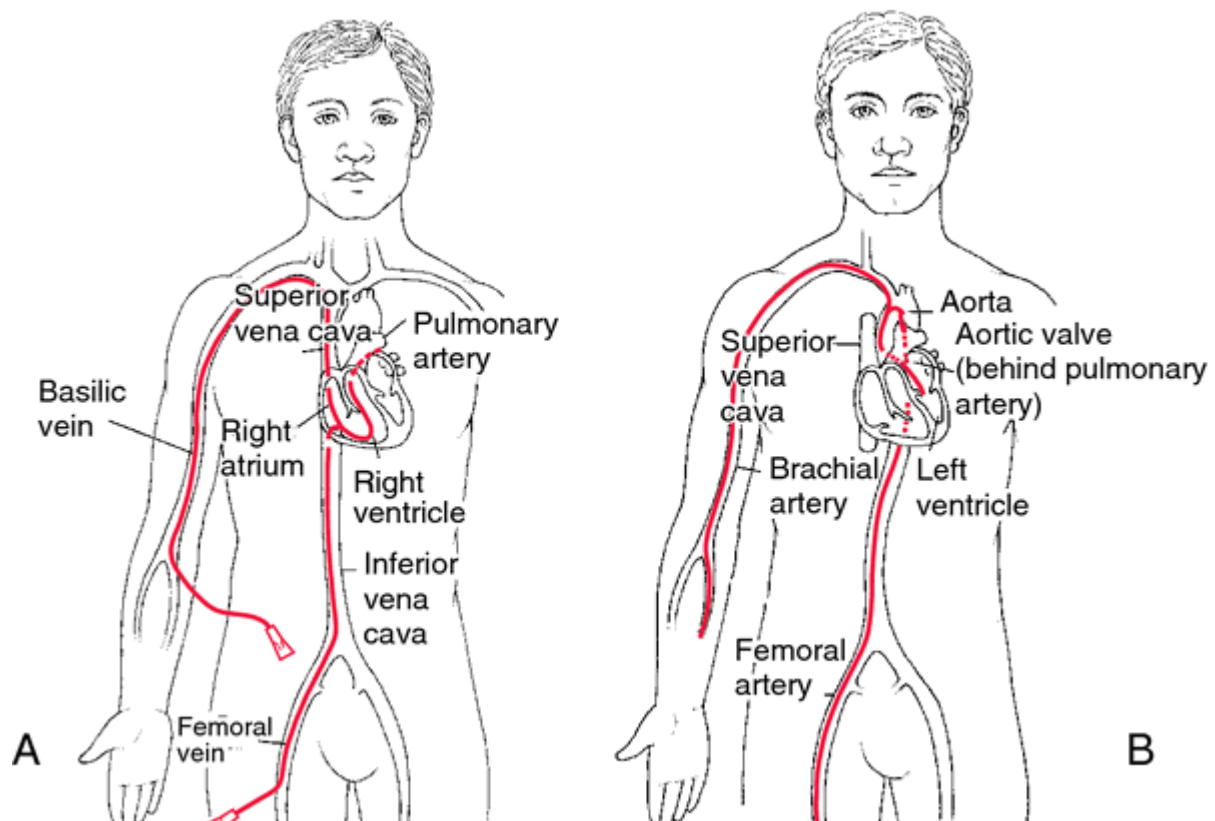


Figure 1.4 A: Catheterization of the right side hearth cavities or pulmonary artery. The catheter is inserted into the femoral vein and advanced through the inferior vena cava, or, in antecubital or basilic vein, through the superior vena cava. B: Catheterization of the left side hearth cavities or aortic artery. The catheter is inserted into the femoral artery or the antecubital artery and advanced through the aortic different portions.[4]

Catheterization can also have a treatment use besides the diagnostic one. Good example of that are the heart valves replacements or the stent placement in a coarctation in elastic arteries. The combined catheterization for pressure measurements and stent implantation has been widely used in the management of both native and recurrent coarctation of the aorta in adolescents and adults, reducing the number of cardiovascular surgery. This procedure has a high success rate (around 90%).[22] However, since this is an invasive procedure, complications like femoral access vessel related, aneurysm formation, aortic dissection, and cerebrovascular accident can occur that in rare cases can even be fatal (0.3%).[16] Also the stent placement or cardiovascular surgery is only made when there is reduction of the gradient to less than 20 mmHg.[16] Thus, there are cases a catheterization is made but no intervention is needed, which increases the patient risk of further complications.

Nevertheless, given the well-established accuracy of pressure measurements, for medical decision making cardiac catheterization is still considered the clinical gold standard despite its known drawbacks concerning invasiveness, ionizing radiation exposure and costs.<sup>5</sup>

### 1.2.2 Angiography

First developed in University of Lisbon by Egas Moniz [23], angiography is an exam, traditionally fluoroscopic, where the blood or lymphatic vessels are imaged. This is possible by injecting a radio-opaque contrast media into the vascular system in order to get a higher contrast to X-rays between the vessels and the involving tissues, providing a 2D image of the vascularity intended.[24] It is mainly used for diagnosing a great variety of CVD where there is stenosis or enlargement of the vessels. Since it is relatively expensive and has inherent risks due to the ionizing radiation used in this modality, its use is decided according to a normative that evaluates its cost/benefit patterns.[25]

Nowadays, less invasive angiography techniques are being researched and developed for vascular imaging, such as Computed Tomographic Angiography (CTA), or Catheter Arteriography. For instance, there are already studies supporting the possibility of getting some information from blood flow velocity using CTA [26, 27], or stress myocardial perfusion.[28]

### 1.2.3 CT

Multi-slice cardiac computed tomography (CT) is a rapidly advancing technology that is being used for imaging the cardiovascular structures such as the heart and the vessels. Due to its inherently high spatial resolution (enabling isotropic data acquisition), fast scan speed, and tissue contrast (that can be increased by using a contrast agent), Multi-slice CT has been used in diagnosing and treatment planning of CVD. For example, it is used in the evaluation of the complete coronary vascularity or, more specifically, the aortic valve structure. As this is mostly an anatomical analysis method, there is currently no known research in CT technology specifically focusing on calculating the blood flow velocity. However there are studies that calculate a mean of the blood flow velocity by using contrast agents to reach other goals such as the xenon solubility coefficient in the human liver or regional cerebral blood flow differences in order to evaluate the risk of Alzheimer's disease.[29]

### 1.2.4 PET

Cardiac Positron Emission Tomography (PET) is also increasingly being applied clinically, mainly through myocardial perfusion imaging which evaluates heart muscle function over time as well as the way blood is flowing into the myocardium.[30] Compared with CT, PET offers lower radiation exposure, fewer artefacts, improved spatial resolution, a great variety of available radioisotopes, and, mainly, an improved diagnostic performance. However, the cost of



the machinery and the exams are a big issue and additional studies are necessary to further validate cost-effectiveness and also the real relative diagnosing impact of PET.[31]

It is important to notice that all of these first 3 modalities (fluoroscopic angiography, CT or PET) involve the exposure to ionizing radiation, and therefore they all present health risks.[32-34]

### 1.2.5 Echocardiography

This non-invasive technique is based on ultrasound and echo wave physics, offering an easy and fast assessment of cardiovascular

components. Since it is harmless and non-invasive, can provide real time images which can focus either or both function or anatomy of the cardiovascular components it is the most commonly used cardiovascular modality in general clinical practice. Images can be acquired in 2D, 3D, and even in 4D which are 3D image sets that are

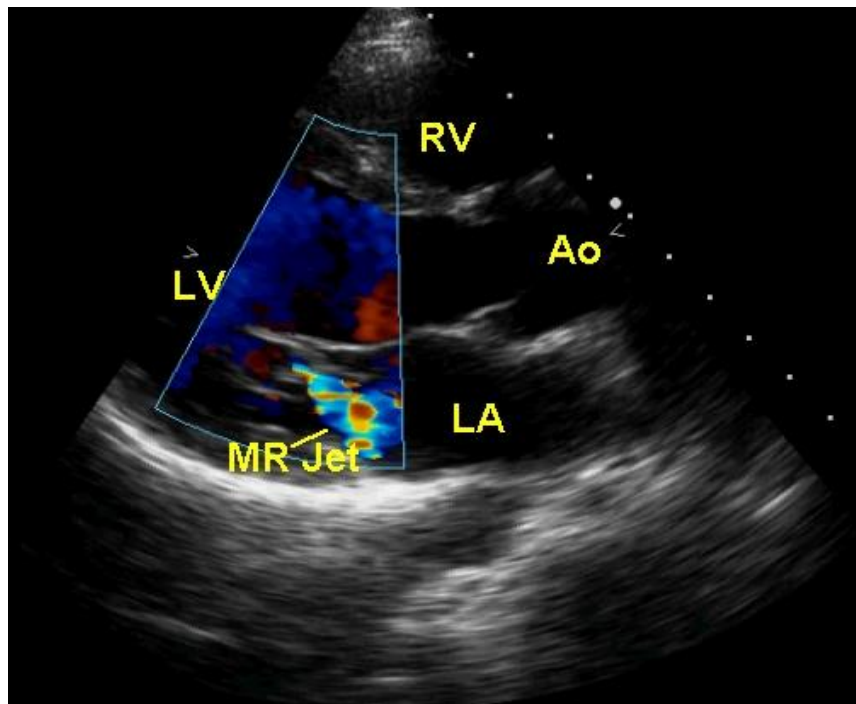


Figure 1.5 Colour Doppler echocardiogram in parasternal long axis view showing mitral regurgitation (MR jet), the heart cavities: left ventricle (LV), left atrium (LA), right ventricle (RV) and aorta artery (Ao).[1]

acquired and displayed in real time.[35] For the blood flow analysis, however, the most important aspect of echocardiogram is the 2D colour Doppler imaging (see Figure 1.5). The also named Doppler sonography is an ultrasound imaging modality that is based on the frequency deviation of the ultrasound wave caused by a reflector in motion[36], in the case of Echocardiography, Blood. The most common use of Doppler echocardiography is based on the duplex scanning imaging, which is a combination of the ultrasound images, two-dimensional B-mode, and the images resulting from Doppler that are superimposed on the two-dimensional image of B-mode. This combination allows a very complete picture, since the B-mode two-dimensional image of grey scale allows to distinguishing the different anatomical structures and the images resulting from the Doppler techniques originate from a colour gradient for assessing the blood velocity.[36] Therefore Doppler echocardiography is a method for assessing the size, thickness and movement

of various cardiac structures and blood that circulates in them. This enables the diagnosis of a variety of diseases such as congenital defects[37], hypertrophic cardiomyopathy[38], coronary artery disease[39, 40], intracranial occlusive disease intracranial occlusive disease [41] or the determination of systolic and left ventricular diastolic functions [42, 43], among others. However, when applied to measure the severity of a stenosis in the aorta, the Doppler echocardiography tends to overestimate the aortic pressure gradient and measurements are sometimes difficult to obtain due to the posterior position of the aorta, particularly in the adult patient.[8, 44]

### 1.2.6 Hybrid imaging

Besides the use of individual CVI focusing on a single objective, the potential of using cardiac hybrid imaging has also been studied. Hybrid approaches may in some cases allow a more comprehensive diagnosis of CVD since it becomes possible to combine both morphological and functional information.[45, 46] The goal is to obtain a more accurate and less/non-invasive imaging scan that can be used in diagnosis and/or treatment planning. Applications for blood flow analysis are under research, using hybrid methods such as the fusion of PET and CT[47, 48], PET and MRI [49, 50], either CT or PET with CTA [46, 51], and photoacoustic imaging, a new biomedical imaging modality that combines high-contrast based on spectroscopic optical imaging with the good spatial resolution of ultrasound imaging.[52, 53]



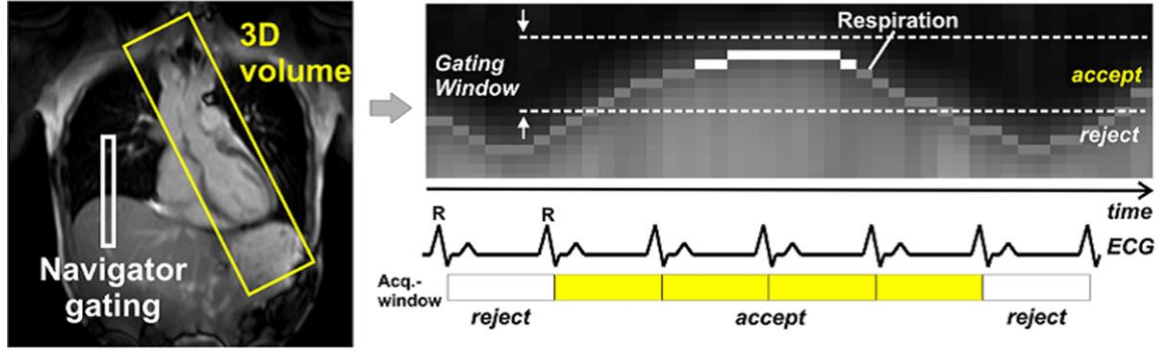
### 1.3 Cardiovascular Magnetic Resonance Imaging

(CMR) provides a more comprehensive evaluation of cardiac physiology and anatomy than Echocardiography. This is possible due to the combination of well-established characteristics of MRI with available approaches for reducing the difficulties caused by heart and breathing motions. MRI is also very flexible regarding the choice of imaging planes, avoiding problems related to the unpredictable anatomical planes of the heart. CMR actually makes it possible to non-invasively view the heart and cardiovascular tree from practically any angular direction, which does not happen with any other imaging technique.[54] CMR also allows as outputs static or cine images.

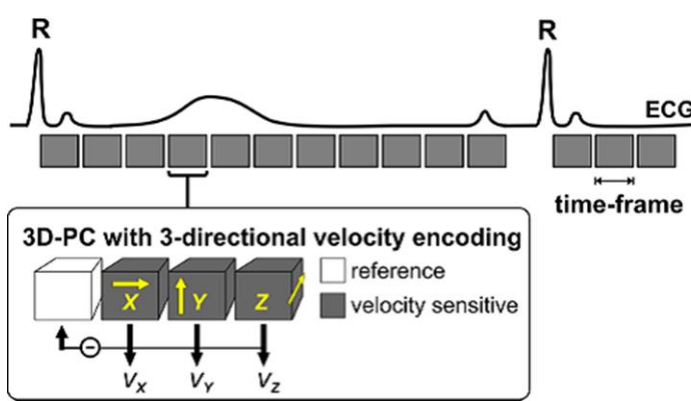
Therefore with a CMR scan it is possible to analyse the cardiovascular anatomy, as well as the function of heart cavities and vessels. As a consequence CMR is suited for visualization and diagnosis of a wide range of congenital and acquired cardiovascular problems, such as coronary artery disease, cardiac insufficiency due to inflammation, or valve problems.[55-59] One of the most important features of CMR is to allow visualizing and quantifying blood flow velocity within the heart and vessels in 3D due to phase contrast MRI and over time (4D) due to the combination of phase contrast MR imaging with the ability of cardiac cine imaging to produce images throughout the cardiac cycle.[60] In order to provide final images which are not affected by artefacts related to respiratory chest movement, this motion must be monitored either using navigators, respiratory bellows or self-gating (see Figure 1.6A).[61] From now on in this dissertation, when mentioning phase contrast MRI (PC-MRI) the inclusion of cardiac cine imaging will be assumed. It is important, at this point to introduce the physics behind PC-MRI.

The applications of gradient pulses induce phase shifts in moving protons that are directly proportional to their velocity along the direction of the gradients. For accurate quantification of phase shift due to moving protons, a reference image is acquired separately so that phase shifts induced by other uncontrollable factors, such as magnetic field inhomogeneities, can be subtracted to from the pulse induced images (see Figure 1.6B). Repeating the acquisition for 3 orthogonal directions, it is possible to obtain phase maps which encode velocity ( $V_x$ ,  $V_y$ ,  $V_z$ ), with phase shifts within the range of  $\pm 180^\circ$ . This means that, for each pixel, the measured phase (RAW format) depends on the velocity of the spins. As a result, stationary protons appear grey, spins which flow in the direction of the sensitising gradients appear brighter, and spins which move in the opposite direction appear darker (see arrows in Figure 1.6C). The peak velocity encoding (VENC) value is defined by the user.

### A: Respiration Control (navigators, bellows, self-gating, ...)



### B: ECG gated flow-sensitive 4D MRI



### C: Raw Data

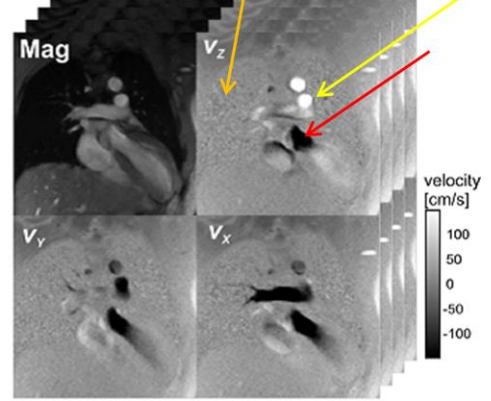


Figure 1.6 A: Data acquisition for 3D cine velocity acquisition using navigator gating for respiration control. The navigator gating control is placed above the lung and establishes a gating window for image acquisition. Therefore not all the heart beats are considered when acquiring PC-MRI images. B: Schematic illustration of ECG-gated three-directional phase-contrast MR (3D-PC) sequence used to measure blood flow. Velocity encoding was performed using four modules: a reference module and one for each of the 3 different velocity directions  $V_x$ ,  $V_y$  and  $V_z$  per time frame, also known as time step, (1 time frame establishes the PC-MRI time resolution). X, Y, and Z are the three (slice-select, phase-encode, and frequency-encode) gradient axes used. C: Raw data per slice and per time frame obtained from the four velocity vector extraction (One Magnitude image and different velocity components  $V_x$ ,  $V_y$  and  $V_z$  velocity images). In this image it is possible to verify that stationary protons appear grey (orange arrow), flow in one direction appears white (yellow arrow), and flow in the opposite direction appears black (red arrow)[6]

The amplitudes of the flow-sensitizing gradients are calculated so that the peak velocity encoding (VENC) is defined by the user and corresponds to a phase shift of  $180^\circ$ . Given this, the velocity,  $v$ , within each voxel can then be determined by the mean of the protons phase difference,  $\Delta\Phi$ , accrued during one time step (temporal resolution), using the formula:

$$\Delta\Phi = \gamma * \Delta m * v$$

where  $\gamma$  is the gyromagnetic ratio and  $\Delta m$  denotes the difference of the first moment of the gradient-time curve. The closer the VENC is to the maximum expected velocity (ideal VENC), the more precise is the measurement. Therefore there are clinical guidelines for Venc determination. Some these values are presented next[62]:

- Venc setting for normal aorta : 200 cm / s
- Venc setting for aortic coarctation : 400 cm / s

- Venc setting for normal mitral valve : 150 cm / s
- Venc setting for mitral stenosis : 300 cm / s
- Venc setting for normal tricuspid : 100 cm / s
- Venc setting for tricuspid stenosis : 200 cm / s

It is important to notice that if VENC is set too low compared to the maximum blood flow, velocity encoding results in aliasing or phase wrap (also known as wrap-around) as indicated by an inverted signal flow where the intensity signal has a maximum brightness correspondent to phase shifts very close to  $\pm 180^\circ$ .

Another problem when a very low VENC setting is selected is that the entire flow information in the background will present significant levels of noise. Another problem is that setting a low VENC implies using stronger gradients to cover the same phase interval ( $\pm 180^\circ$ ), and so stronger Eddy currents are induced when the gradients are switched on or off.[62] Nevertheless, it has been reported that if the VENC is set at no more than three times the ideal value, the peak velocity measurements show deviation less than 10%, a clinically acceptable level of error.[63] Other sources of in PC-MRI acquisitions other than inadequate VENC values include deviation of the imaging plane during data acquisition (e.g., cardiac or respiratory motion), inadequate temporal or spatial resolution, and field inhomogeneity (e.g., susceptibility artefact from metallic implants). Therefore, depending on the structure of interest, PC-MRI parameters should be set in order to minimize potential sources of error.[64]

Several image data sets can be acquired from of PC-MRI by processing the RAW data[62]:

- Phase images presenting the actual 4D flow measurement with a grey background correspondent to the stationary tissue. The positive flow (coinciding with the gradient direction) is presented in white while the negative flow will be black;
- Magnitude reconstructed images which represent pure anatomical information regarding the structures where the blood flows
- Re-phased images representing reconstructed image from the RAW data with anatomy and flow emphasis. This kind of image, known as phase contrast magnetic resonance angiography (PC-MRA), provides the flow velocity profiles and is the type most used in this dissertation. The PC-MRA images can be displayed as maximum intensity projection (MIP) images or as a semi-transparent 3D iso-surface which can be combined with 3D flow visualization (See Figure 1.7).

Velocity and flow information can be obtained using commercial softwares that allow the user to define 2D or 3D ROIs in the vessel's lumen or within an intracardiac region sampled throughout the cardiac cycle. It is therefore important to understand the acquisition, visualization and quantification of these image sets as well as the potential applications of PC-MRA.

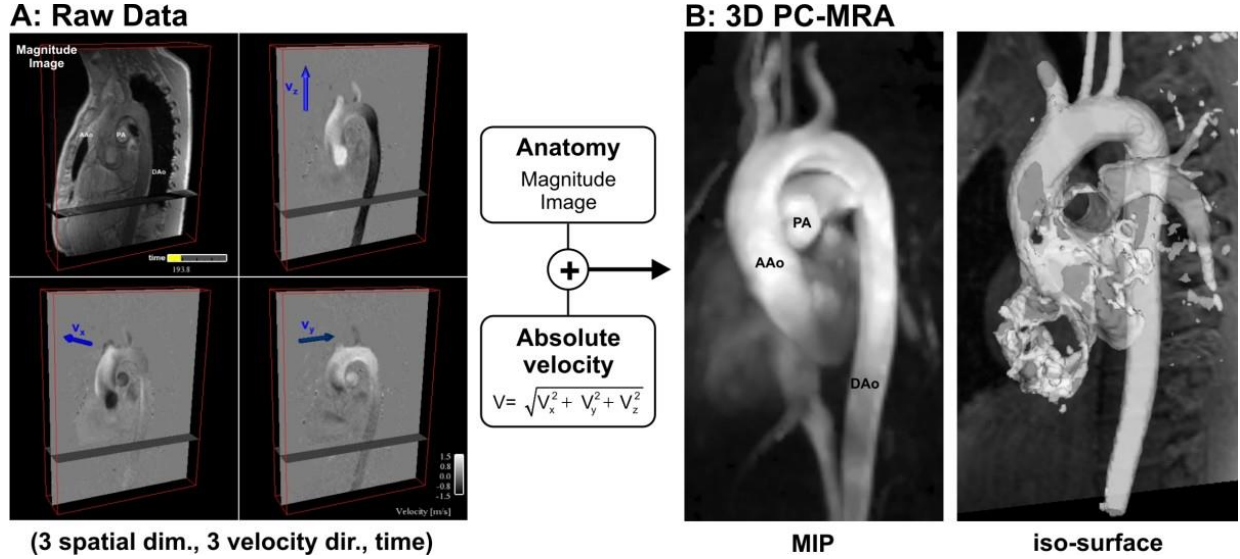


Figure 1.7 Image processing for obtaining a 3D PC-MRA of a healthy thoracic aorta. A PC-MRA image is obtained by calculating (voxel by voxel) the absolute velocity resulting from the combination of the 3 different acquired velocity components, with image masking based on the magnitude image. A: RAW data acquired from a PC-MRI with magnitude provided as reference and the 3 different velocity components  $V_x$ ,  $V_y$  and  $V_z$ . B: The resulting PC-MRA images can be displayed as a maximum intensity projection (MIP) or as a semi-transparent 3D iso-surface which can be combined with 3D flow visualization.[6]

### 1.3.1 Acquisition

Although the theoretical principles for 3D and 4D velocity mapping have been known for several decades [65-67], until recently only 2D plane images have been clinically used. These techniques require an operator to correctly align the planes of acquisition and presents other well-known limitations.[68, 69] However, studies have reported that instead of storing the raw information in a 2D segmented k-space, it is possible to store the raw information obtained from the phase contrast gradient echo sequence in a 3D segmented k-space.[70] This allows the combination of 3D spatial encoding, three-directional velocity encoding and CMR cine (4D-VEC-MR) and as a consequence makes it possible to acquire complex 4D blood flow path lines and velocities, which is more notable especially in intracardiac pathologies such as congenital heart defects or acquired valvular diseases.[70]

Unfortunately this type of acquisition takes very long (approximately 10 minutes for a whole heart 4D measurement on a 1.5 Tesla MRI scanner) as it is necessary to synchronise the image acquisition with the respiratory and cardiac movements.[71] In other to reduce the

acquisition time while avoiding artefacts, it is common to use ECG triggers as illustrated in Figure 1.6B) [6] and monitored by CMR navigators [72] (Figure 1.6A) or self-gating techniques.[73] The consequences are that actually 30 to 60 % of the acquired data is rejected, depending on the regularity of the respiration and also on the existence or not of arrhythmias. The efficiency can be increased and the overall scan time reduced by changing the acquisition strategy. One option which is under investigation is the use of spiral k-space trajectories (spiral 4D flow).[74]

### 1.3.2 Pre-processing and PC-MRA calculation

In order to avoid offset errors in PC-MRA calculation due to Eddy Currents or phase wraps it is necessary to do a pre-processing step before analysing the 4D data. This Pre-Processing step consists in two parts: in the first part the non-moving tissues surrounding the heart are excluded, based on a low intensity tissues detected by the PC-MRI. This leads to a reduction of the Eddy Currents artefact. Secondly, it is applied an algorithm that proceeds to phase unwrapping in a small area with phase wraps in one of the phase encoded vector fields (in the tool used during this project, this feature was not fully operational). This step must be adapted to the CMR system, protocol and anatomic region of interest (ROI).[75, 76]

After the Pre-Processing, the PC-MRA can be calculated. This calculation allows the identification of vascular boundaries without additional measures. This means that it becomes more intuitive for users to segment blood structures based on contrast between regions where blood is circulating versus regions where there is no blood in circulation. In the case of the heart, its boundaries are in constant movement through the cardiac cycle. Since, in the calculation of PC-MRA, the cavities wall motion is not included, the ventricle's boundaries estimated from the PC-MRA correspond to a mean of the wall position and are therefore smaller than the maximum volume of the ventricle in diastole.(Figure 1.7B).[6]

### 1.3.3 Data analysis

The first aspect when processing 3D CMR blood flow images is getting a visual image of the blood flow (pathlines and/or streamlines), the velocities vector field, and with some softwares the connectivity map or the blood flow pressure maps.[77]

It is important to quantify the visualized parameters regarding blood flow measurements. Based on PC-MRA data sets it is possible, with the appropriate software tools, to obtain the following measurements:

- Evaluation of blood flow, velocity, area of specified ROI's [78];
- Pressure differences [77, 79];
- Wall shear stress [80];
- Vessel elastic properties [81];
- Turbulence intensity.[82]

Given the potential of 4D velocity acquisition, several studies have been emerging in order to associate characteristics of the blood flow in the heart and big vessels with the diagnosing and analysis of the progression of a cardiovascular disease or condition that might change the blood fluid dynamics.[83, 84]

## **1.4 Blood Flow Imaging state of the art**

As there are so many different Cardiovascular Imaging (CVI) techniques and sub-techniques, it cannot be said that the global state of the art is dominated by a single CVI modality. Instead, It is useful to consider the state of the art for each different measurement that can be made. This work will only focus on the state of the art of blood flow analysis.

Even considering that CT provides fast 3D anatomical scans with very good spatial resolution, being able to detect the propagation of a contrast agent over time, it still does not provide more than an approximate estimate for the velocity of blood flow. As a consequence this is not the best imaging technique for blood flow analysis.

Alternatively, Doppler echocardiography can be employed to directly measure regional blood flow velocities in a 2D plane. Therefore this is the imaging modality which is more widely and routinely used for blood flow analysis and pathology diagnosing. When compared with CMR, and more precisely with PC-MRI this modality has some advantages that include the scan price and time, the amount of detectors available and the fact that it can be used in patients with pacemakers or metallic implants. It is also the best method to specifically image the exact location of one of the heart valves due to the thinner and more mobile leaflets compared with 4D CMR velocities mapping.

However, Doppler ultrasound does not allow the measurement nor the detection of non-regional blood structures in a single measurement as possible with CMR. It is also not possible to obtain 3D images. Studies have also shown that with Doppler ultrasound, peak velocities can be overestimated by as much as 25%.[85] Mean flow in large vessels can also be overestimated due to assume as constant velocity over the whole vessel area. In contrast, with PC-MRI it is possible to measure the variation of flow within the vessel. PC-MRI therefore has been found superior to

Doppler sonography for evaluation of mean flow.[86] In fact, CMR still has other potential advantages such as the retrospective analysis of the blood flow at any location and in any direction within the image volume. Further possibilities include measuring shear rates, pressure gradients, turbulence or even blood flow KE. However, the use of CMR compared to other techniques has some drawbacks including the long duration of the CMR 4D exam and complicated postprocessing, the moving boundaries of the heart cavities and the limited knowledge available. Therefore, before real clinical diagnosing and predictive value of flow measurements can be established, there is still the need for further investigation, including large studies with imaging performed before and after interventions, therapies or following the progression of different conditions.[6] Solutions to overcome the extensive duration of the 4D blood flow velocity mapping are currently under research and include:

- Combination with other image techniques such as echo-planar imaging and radial imaging [87, 88];
- Gaining signal-to-noise ratio (SNR) by using higher CMR magnetic fields such as 3T or 7T.

## 2 Objectives

### 2.1 Software Refinement

Flow analysis based on PC-MRA is a recent research area which is currently being explored. Therefore it is natural that there not yet available on the market extensively tested softwares; as a consequence, when using the ones that are currently available on clinical datasets, problems naturally arise which require tweaking the software. This is actually the main reason for the establishment of cooperations between developers and researchers which allows the development of better softwares/analysis tools and also the increase of knowledge on this research area.

In this project the MevisFlow software for blood flow analysis based on PC-MRA was mostly used. A more detailed description of this software is provided in the Material section (4.2.1). In order to reduce problems that could appear when developing the project, and also to have a better accuracy in the results, testing and refining this analysis tool from a clinical point of view was set as a first objective. The aim was to use all the relevant features of the program on a selected group of PC-MRA datasets, representative of the type of data analysed within this project. When problems or missing measurements were detected, an analysis of the causes was made and the information (screenshots, videos or working directories) sent to the developers in order to correct any problems and/or include new measurements. This interaction was stronger at the beginning of the project, but it also extended throughout the whole duration of the project.

### 2.2 Pressure gradient across an aortic coarctation

Cardiac Magnetic Resonance (CMR) provides high-quality anatomic information of the aorta. However, flow velocities using 2-dimensional velocity encoded cine magnetic resonance imaging (VEC-MRI) were reported to underestimate pressure gradients.[89] Four-dimensional VEC-MRI (4D-VEC-MRI) provides time resolved blood flow velocities in a 3-dimensional volume that can cover the entire aorta. From these velocity fields, dynamic pressure differences along the course of a vessel (4D pressure fields) can be computed by solving the Pressure-Poisson equation.[90-93] Briefly, the Pressure-Poisson equation is derived from the momentum equation of the Navier-Stokes equations for incompressible fluids by applying the divergence operator. The



validity of 4D pressure fields has been systematically evaluated on phantom and initial human studies.[90]

The goal of this study was to investigate the accuracy of this method in a clinical setting in patients with CoA. In this context it was investigated the agreement between VEC-MRI based 4D pressure fields and cardiac catheterization as the clinical gold standard.

## **2.3 Kinetic energy within the ventricles**

One of the possible measurements that can be made from PC-MRA is actually the Kinetic Energy (KE) and the KE loss, which has the potential to become an important measurement to consider in future diagnosing and follow up of pathologies, especially within the heart. Actually The question of the maintenance of KE of blood flowing in the heart, forming loops, within the heart by loops has been recently been under discussion [94, 95], but it is commonly agreed that it this issue is connected with flow inertia.[96] Therefore the first attempts to have an idea about investigate KE within the heart was by studying invasively the pressure decay of LV and from then measure the inertia force.[96, 97] Up to now, a single study has been carried out in order to non-invasively visualize and quantify the KE within the ventricles using CMR.[5]

The main objective of the present study is to visualize and to quantify the amount of KE lost within the ventricles (both LV and RV) and to compare the energy curves of healthy ventricles with patients with conditions in the respective valve (Mitral valve in the LV study and pulmonary valve in the RV study). Since this is a blood flow parameter that has not been explored [5], the software used does not allow a direct KE measurement. It was therefore necessary to develop a procedure in order to accurately calculate the KE more quickly and in a more direct way. It was then necessary to collect datasets from both patient and control groups and analyse the results. The last objective within this topic was to create distributions and comparison curves to facilitate the visualization of the results.

## **2.4 Other objectives**

In order to complement the main objectives while taking advantage of the available data sets, other objectives were also defined, involving collaboration with other members of the team:

- To compare and understand the differences on the amount of KE lost in LV and RV.

- Analyzing the path followed by the blood flow within the RV in one or more heart beats through visualization and quantification;
- To build moving models of the full heart based on acquired MRI images.

### 3 Work's planning

In this chapter the materials used and the collaborations established during this project are briefly described and explained. For easier reference, the planned tasks in this Master Thesis project are presented on Table 3.1 ordered by dates:

Date	Task
1 to 12.10.2012	Creation of image database from pre- and post- operation MRI scans of patients with mitral valve conditions for left ventricle kinetic energy (LVKE) study (the exams had been previously performed).
15 to 25.10.2012	Familiarization with MevisFlow cardiovascular MRI postprocessing imaging software
25 to 26.10.2012	Brief comparison between MevisFlow and other blood flow analysis softwares (mainly with GTFlow)
29.10 to 07.12.2012	Testing of MevisFlow software on a group of image sets in order to detect potential bugs
06.11.2012	1st Meeting with the biomechanical fluid specialist from Biofluid Mechanics Lab in Charité Universitätsmedizin Berlin
27.11 to 07-12-2012	Theoretical description of kinetic energy calculation from velocity vector fields
14.11.2012	1st Meeting with MevisFlow developing team in Fraunhofer MEVIS Bremen
10.12.2012 to 26.01.2013	Introduction to MevisLab medical imaging programming software and CAIPI medical imaging postprocessing software
12.12.2012	2nd Meeting with MevisFlow developing team members in German Heart Institute Berlin
21.01 to 30.04.2013	Scanning of healthy volunteers for the LVKE study
21.01 to 07.02.2013	Development of MevisLab algorithm for calculation of kinetic energy (KE) within a previously segmented volume

08.02 to 22.02.2013	Development of a procedure combining MevisFlow, CAIPI (for 3D left ventricle segmentation) and MevisLab KE calculation algorithm
18.02.2013	Finalisation of MevisFlow version with majority of the detected bugs corrected
25.02 to 01.03.2013	Testing of KE procedure on several image sets
01.03 to 30.06.2013	Application of the KE procedure to all LVKE study patients and volunteers
06.03 to 13.03.2013	Idealization of a MRI non-invasive aortic pressure measurement study in patients with CoA
14.03 to 21.03.2013	Creation of image database for pressure study patients (from MRI previously scanned patients)
22.03 to 24.05.2013	Segmentation of the aorta and creation of the respective pressure maps (Data acquisition)
01.07 to 01.08.2013	Statistical analysis and discussion of the results of both studies: Pressure gradient and LVKE
until 27-09-2013	Submission of master thesis Dissertation for later presentation

Table 3.1 Work plan of the project by expectable dates and tasks.

### 3.1 Collaborations

This project was developed at a hospital as part of a medical and research team who focuses on blood flow analysis and CMR scanning patients, mainly children, teenagers or adults with possible or already diagnosed cardiovascular congenital diseases. As datasets were readily available, there was no need to establish further collaborations to provide the data required for this study.

However it was very important to establish collaborations with software programmers as well as mechanical fluid specialists.

#### *MevisFlow developing team*

The collaboration established with the MevisFlow developing team was of the outmost importance to this project, since their tool allow or, at least have the potential to analyse the blood flow within ventricles including almost all parameters of interest.

On the other hand, this team is part of Fraunhofer MEVIS, the company that developed and works with MevisLab, which means that the team's experience working with this program could be very important to the correct implementation of new algorithms.

This collaboration was also beneficial from the MevisFlow team point of view, once it allowed other users to identify new needs which could help to further develop the program.

#### *Biofluid Mechanics Lab Specialist*

The Biofluid Mechanics Lab of the Charité Universitätsmedizin Berlin, and more in concrete this Biomechanics specialist, Leonid Goubergrits, has a long time partnership with the team, being a fundamental piece in much of its research projects. In this project it is important to keep contact with him since he has more expertise on what is possible and viable to do within this time period and also to give feedback on how the best way is in order to calculate KE and KE lost

The Biofluid Mechanics Lab of the Charité Universitätsmedizin Berlin, and more specifically this Biomechanics specialist, Leonid Goubergrits, has a long time partnership with the team, being a fundamental piece in much of its research projects. In this project it was important to keep contact with him, as his expert knowledge was essential to evaluate what was possible and viable to do within this time period and also to get feedback on how to best calculate KE.

## 4 Material

### 4.1 CMR Scanner

The CMR study was conducted on a whole body 1.5 Tesla MR scanner (Achieva R 3.2.2.0, Philips Medical Systems, Best, The Netherlands) using a five-element cardiac phased-array coil (Philips Medical System, Best, The Netherlands).

*Blood flow:* Three directional blood flow velocities were measured over the cardiac cycle using anisotropic k-space segmented 4D-VEC-MRI with retrospective electrocardiographic gating.[98] As previously validated, blood flow can be quantified accurately in aortic pathological flow conditions using 4D VEC MRI.[99] The acquired volume covered the thorax from the apex of the heart to the aortic arch in the feet-to-head direction, the external border and spine in the anterior-to-posterior direction, and the ascending and descending aorta in the right-to-left direction. Example scan parameters of this sequence were: field of view feet-head 180 mm, anterior-posterior 200-230 mm (depending on the patient size), right-left 90-105 mm (depending on the number of slices used), , acquired voxel  $2.5 \times 2.5 \times 2.5 \text{ mm}^3$ , reconstruction matrix  $128 \times 128$ , reconstructed voxel  $1.7 \times 1.7 \times 2.5 \text{ mm}^3$ , flip angle  $5^\circ$ , shortest repetition and echo time (traditional values were echo time 1.1 ms, repetition time 3.2 ms), nominal temporal resolution varying with heart rate for 25 cardiac phases, velocity encoding 400 cm/s for aorta and 150 cm/s for ventricles within KE study.

*Anatomy:* 3D anatomy of the aorta was determined using a clinically established contrast-enhanced MR angiography method. The injection dose of contrast agent containing gadolinium (Dotarem®, Guerbet, Villepinte, France) was 0.2 ml/kg of body weight corresponding to 0.1 mmol gadoterate meglumine/kg of body weight. The typical used sequence parameters were: echo time 1.1 ms, repetition time 3.2 ms; flip angle  $30^\circ$ , field of view 510 mm; parallel imaging with an acceleration factor of 2 (SENSE); and half-Fourier acquired voxel size,  $1.2 \times 1.2 \times 2.2 \text{ mm}^3$  (reconstructed to  $0.9 \times 0.9 \times 1.1 \text{ mm}^3$ ).

## 4.2 Postprocessing softwares

In order to fulfil the objectives of this project it was necessary to use some medical imaging softwares in order to perform the correct blood flow analysis and programming (MevisFlow and MevisLab respectively) as well as a considerable group of MRA image datasets of both patient groups (RV pre- and post- operation and LV pre- operation) and also of a control group.

### 4.2.1 MevisFlow

MevisFlow is a software tool programed in C++ and MevisLab that allows non-invasive interactive exploration of in-vivo hemodynamics. This tool is being developed in cooperation with hospitals and other clinical sites research teams from Germany and USA.[70] It includes panoply of features consistent with the acceptable results provided by well-established techniques like Doppler ultrasound and pressure catheters. The basic function of this software is to calculates the PC-MRA of a DICOM format set of anatomical and 4D flow CMR images, using particle tracing based on images and 3 dimensional blood vessels or structures segmented semi-automatically (watershed segmentation) by the user. This procedure allows the user to visualize and quantify the flow, the velocity vector field and the pressure in either Regions of interest (ROIs) and/or the whole 3D objects. The software interface is divided in 3 main menus that can be seen in Figure 4.1, Figure 4.2 and Figure 4.3.

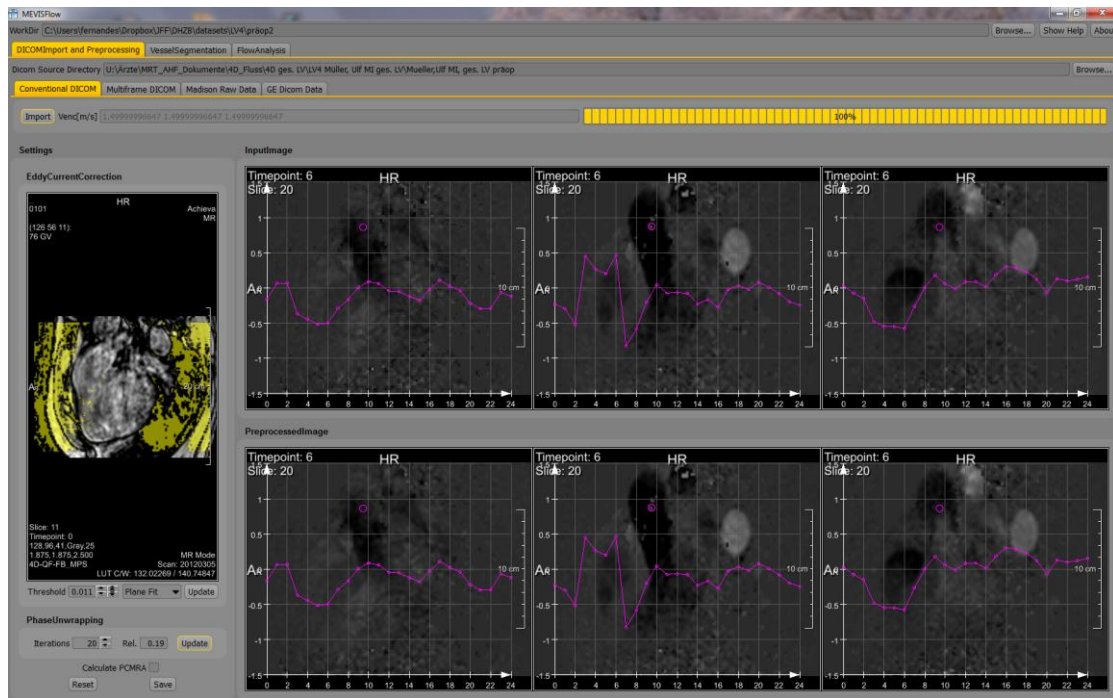


Figure 4.1 Pre-Processing menu, that allows a 4D phase-offset error correction to be made using third-order polynomials (Eddy current correction) as well as a phase unwrapping (still under development). The PC-MRA is also calculated here.

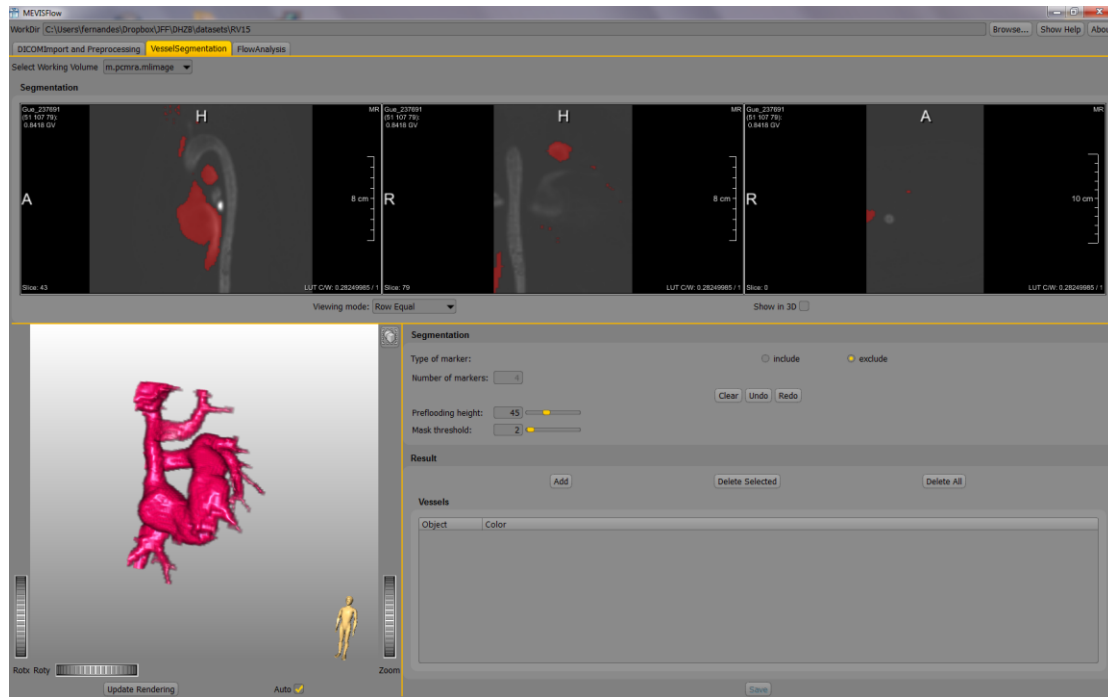


Figure 4.3 Vessel segmentation menu where it is possible to segment semi-automatically (based on markers and filters) several cardiovascular structures for the same image set.

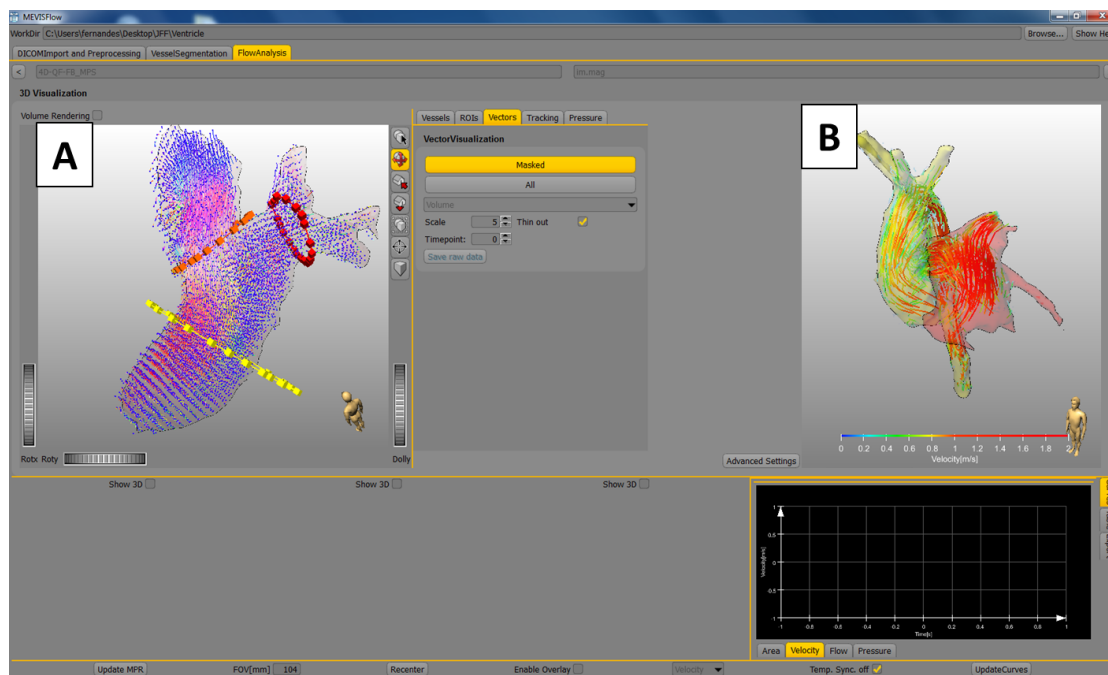


Figure 4.2 Flow analysis menu, where it is possible to draw and select the ROIs, visualize and export vector fields (A), tracking particle flow or pathlines (B), visualise the connectivity map, compute and visualize the blood flow pressure, and see and export the temporal evolution of the vessel cross-sectional Area, velocity, blood flow and pressure for a single cardiac cycle.

Since this software was of outmost importance in the development of this master thesis project and is still under development, the MevisFlow software was tested on 10 image datasets. For these datasets, both LV and RV were segmented and complemented with some information

regarding the aorta and pulmonary arteries. The major bugs are presented in the following Figures and explained in their respective legends.

- Phase Unwrapping Issue (Figure 4.4):

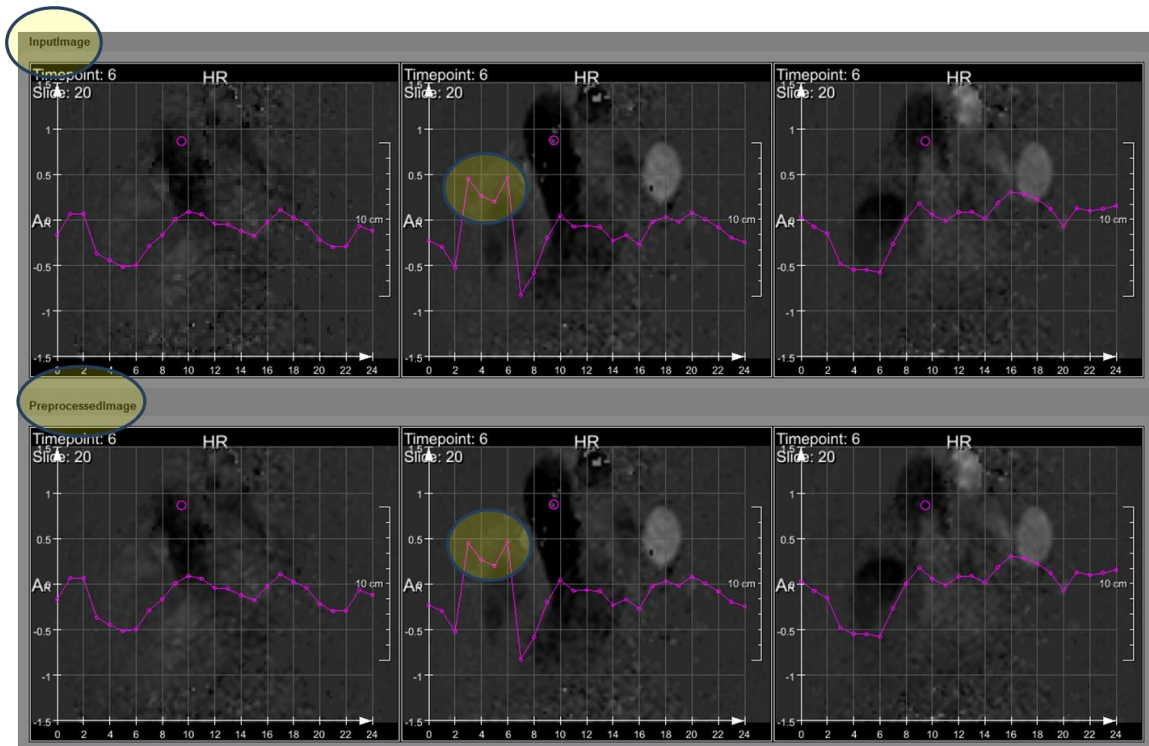


Figure 4.4 After the application of the phase unwrapping algorithm, the phase wrap had not been fully corrected.

- Propagation of the contours over time is incorrectly represented in 3 dimensions (Figure 4.5):

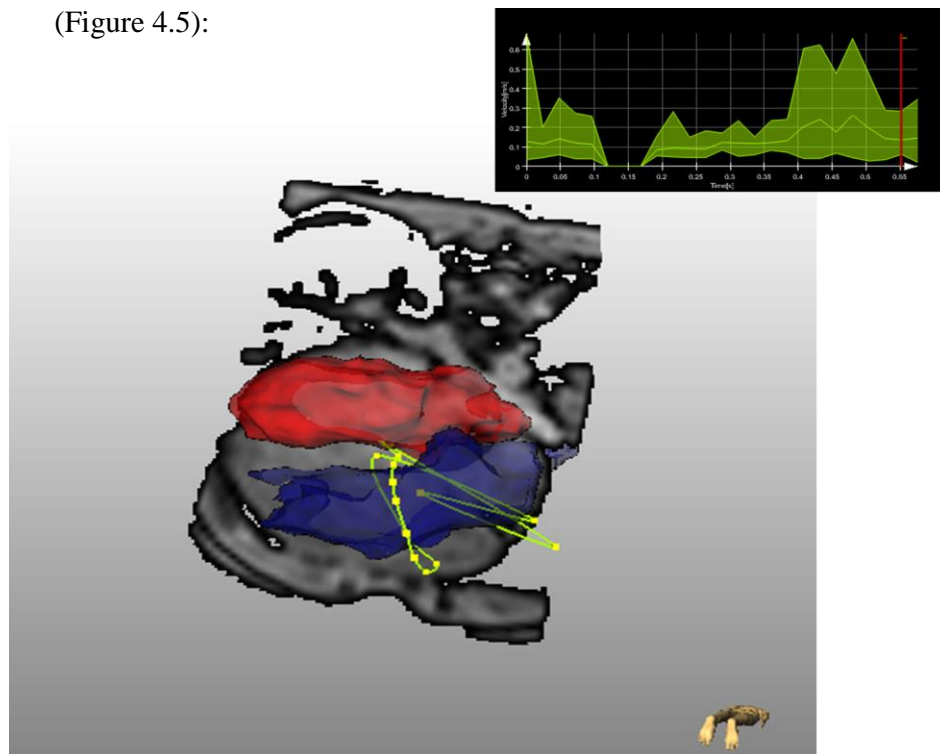


Figure 4.5 An ROI should always be kept in the same plane in which it was drawn. In this and some other cases the contour becomes 3dimensional and as a consequence it is impossible to have information (see graphic above) for a 2D contour in the time steps.



- Particle traces go outside structure (Figure 4.6):

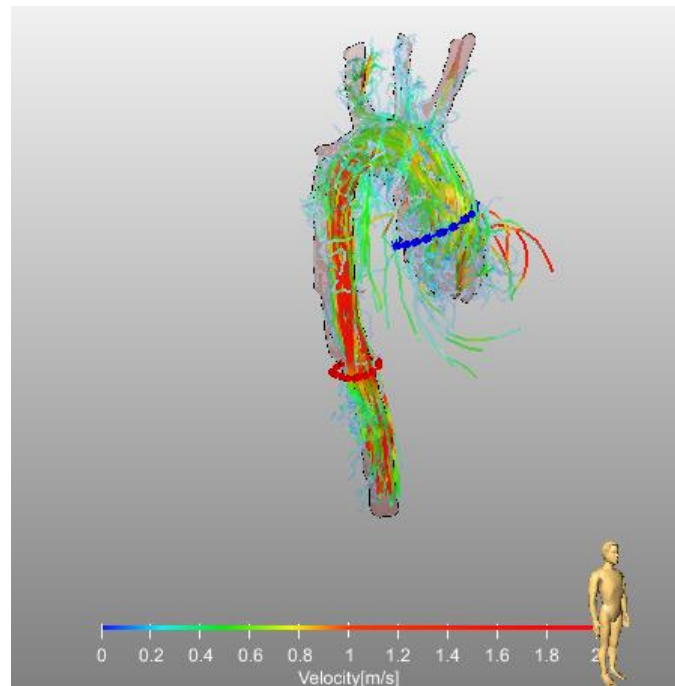


Figure 4.6 The particles emitted went outside the segmented vessel, which can happen because of a bad image acquisition or a bug in the software.

- Issue regarding the colouring of pathlines originating from ROIs (Figure 4.7):

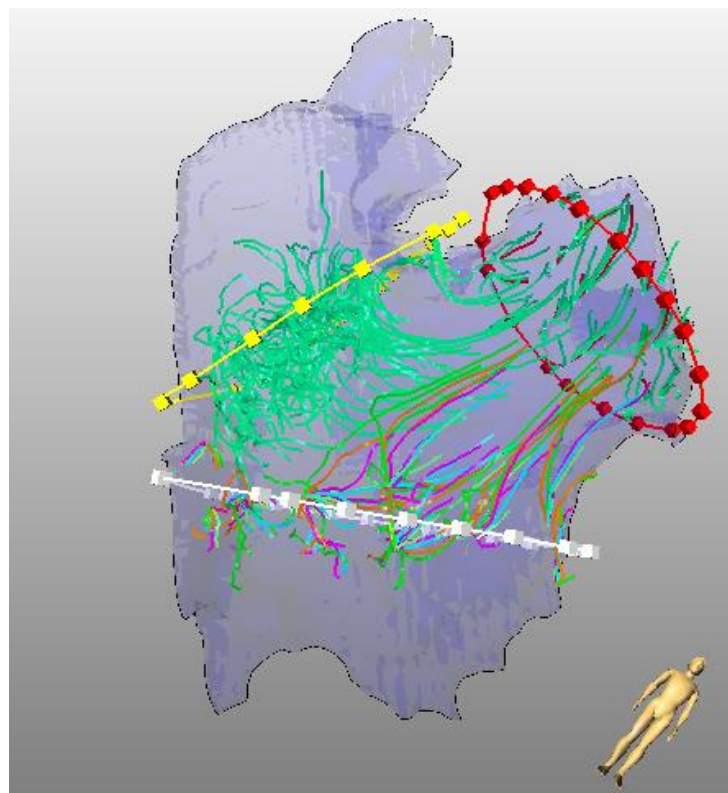
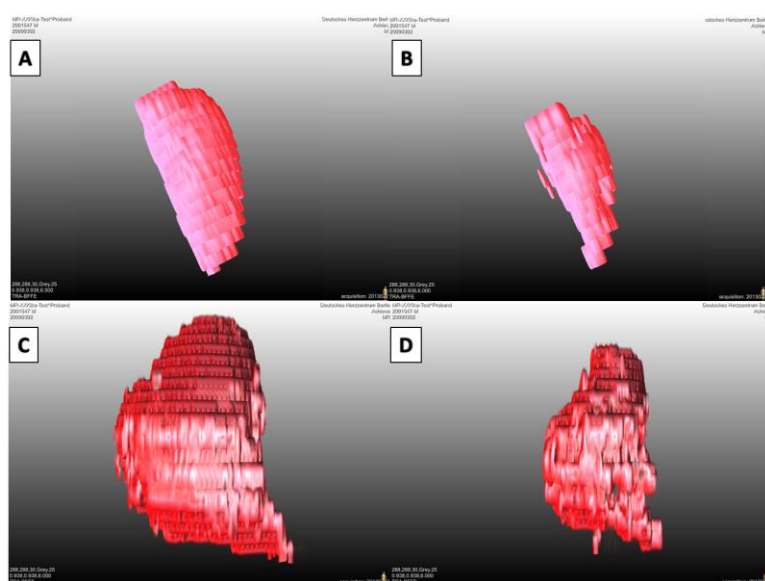


Figure 4.7 When region coloration is used for the pathlines, the colour of the pathlines should be the same as the ROI from which they are originated. In this and some other cases the streamline is either all green or has different colours (similar to what would be obtained if the ID coloration had been used for the pathlines).

However there is still an important issue when segmenting the heart cavities with MevisFlow, as the segmentation corresponds to a static position. This means that only one ventricle segmentation can be made for all cardiac cycle time-steps. Therefore to make an analysis of a moving heart, as in the KE within the ventricles study, it was necessary to consider the complete field of view (FOV) of the PC-MRA image calculated by MevisFlow and make a separately moving ventricle mask using the CAIPI software.

## 4.2.2 CAIPI

A comprehensive analysis of the complex data acquired in an MRI examination plays an important role for differential diagnosis and The CAIPI (Fraunhofer MEVIS) software provides a combined non-invasive analysis and integrated exploration of the relevant CMR imaging data. It includes features as T1 and T2\* mapping, quantification of late enhancement and edema, perfusion analysis, blood pool quantification, analysis of local deformation and synchronized 3D viewing overview with spatio-temporal synchronization of the presented image data, and watershed semi-automatic segmentation. Although this software is still under development in close cooperation with clinical partners from the German Heart Centre in Berlin, it has already been successfully employed in clinical studies.[100]



**Figure 4.8** Moving ventricle masks of healthy volunteers obtained with the CAIPI segmentation tool. A: LV mask of end-diastole (highest blood volume) time step B: LV mask of end-systole (lowest blood volume) time step. The A and B masks were obtained from the same patient and exemplify the moving LV masks set; C: RV mask of end-diastole (highest blood volume) time step D: RV mask of end-systole (lowest blood volume) time step. The C and D masks were obtained from the same patient and exemplify the moving RV masks set. All the masks sets have 25 different masks correspondent to the 25 time steps over a cardiac cycle.

Important refinements were made to the CAIPI segmentation feature in order to suite the KE within the ventricles study here presented. These refinements include the possibility of having a different ventricle mask for different time steps within a heartbeat, allowing a more realistic segmentation of a moving heart as can be seen in Figure 4.8. Another important refinement for more accurate segmentation was the implantation of clip valve planes that avoid the inclusion of regions of the atriums or arteries in ventricle segmentation (see

Figure 4.9). CAIPI segmentation also allows that all the chosen image set to zoom in, center the images and adjust the segmented mask opacity over the anatomical image sets, change the contrast in order to find the best compromise between having an anatomical reference (by visualizing the full heart within each slice for each time step) and a better visualization of the boundaries of the left ventricle.

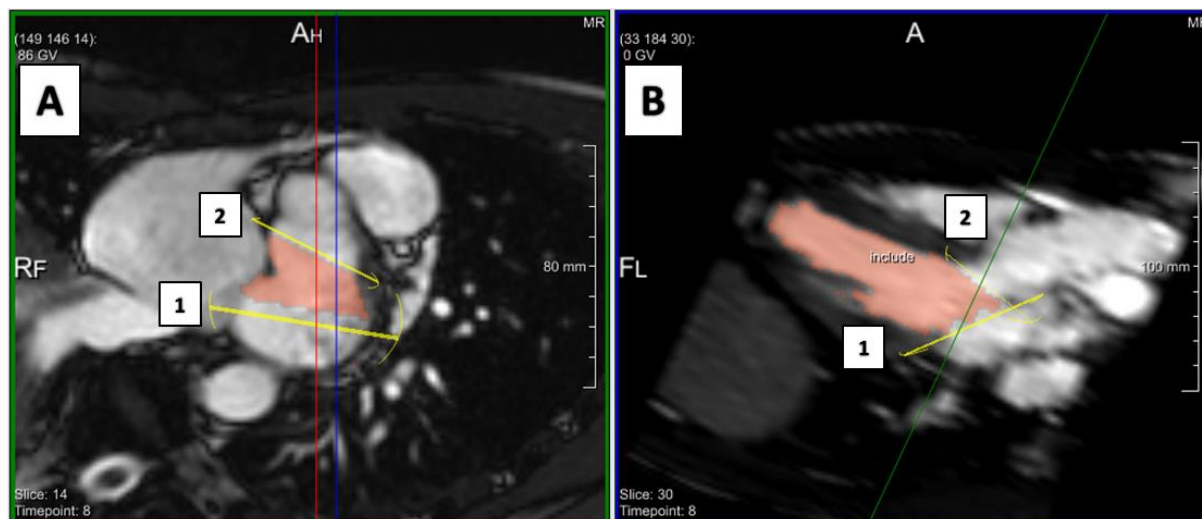


Figure 4.9 Example of valve planes clip on a healthy LV segmentation. The 2 valve planes determined by the user (yellow regions) correspond to the mitral valve (1) and to the aortic valve (2). A: Short axis view of the LV basis, where it is possible to visualize both chosen clip planes. B: Longitudinal view of the LV, where is also possible to visualize the valve clip planes chosen.

### 4.2.3 MevisLab

Also developed in Fraunhofer MEVIS in cooperation between MeVis Medical Solutions AG, MevisLab is a cross-platform tool for medical imaging processing and visualization. For that, this tool includes already advanced algorithms written in C++ and/or python for image registration, segmentation, and quantitative anatomical and functional image analysis, but it also allows the implementation of new algorithms. The software has an open source version as well as a more elaborated licenced one. The module implementation was of outmost importance for the study of KE within the ventricles, as shown in section 6.1.

## 5 Pressure gradient across an CoA study

### 5.1 Methodology

Thirteen consecutive patients (n=7 male, n=6 female, age range 13 to 52 years, mean age  $23 \pm 12$  years) with clinical indication for cardiac catheterization due to CoA and preceding CMR study were included. N=2 patients had native CoA, the remaining had Re-CoA after balloon-angioplasty (n=3 patients) or surgical treatment (n=8 patients). Exclusion criteria were young age that would have required sedation for CMR and general contraindications to CMR. In addition, patients with previous placed stents were did not include in the aorta in order to avoid measurement errors due to susceptibility artefacts and/or radio-frequency shielding.[101]

The study was approved by the institutional research ethics committee following the ethical guidelines of the 1975 Declaration of Helsinki. Written informed consent was obtained from the participants and/or their guardians.

While in the CMR the previously described parameters were used (see CMR Scanner chapter), Cardiac catheterization was done with biplane projection angiographies with Philips Allura Xper FD 10/10 (Philips Medical Systems, Best, the Netherlands) using injection of contrast agent (Ultravist, Schering, Berlin, Germany).

In all patients, catheterisation was conducted under conscious sedation by intravenous administration of a bolus of midazolam (0.1–0.2 mg/kg, max. 5 mg), followed by a bolus of propofol (1-2 mg/kg, as needed) and continuous infusion of propofol (approximately 4 mg/kg/h).

Pressures were obtained in 6 predefined locations along the thoracic aorta before intervention (Figure 5.1A). Pressures were measured with 5-6 French fluid-filled pigtail catheters (Cordis, Warren, USA) that were connected to pressure transducers (Becton-Dickinson, Franklin

Lakes, USA) and amplified, recorded and analysed using Schwarzer Haemodynamic Analysing System (Schwarzer, Heilsbronn, Germany).

Post-processing of 4D-VEC-MRI datasets was done with the software MevisFlow (Fraunhofer Mevis, Bremen, Germany). In a first step, automatic eddy current correction and a phase unwrapping algorithm were applied. Thereafter, the aorta was segmented using watershed 3D segmentation of the lumen.[102]

Pressures were measured by CMR at the same six locations in the aorta where invasive pressures were obtained (Figure 5.1A).

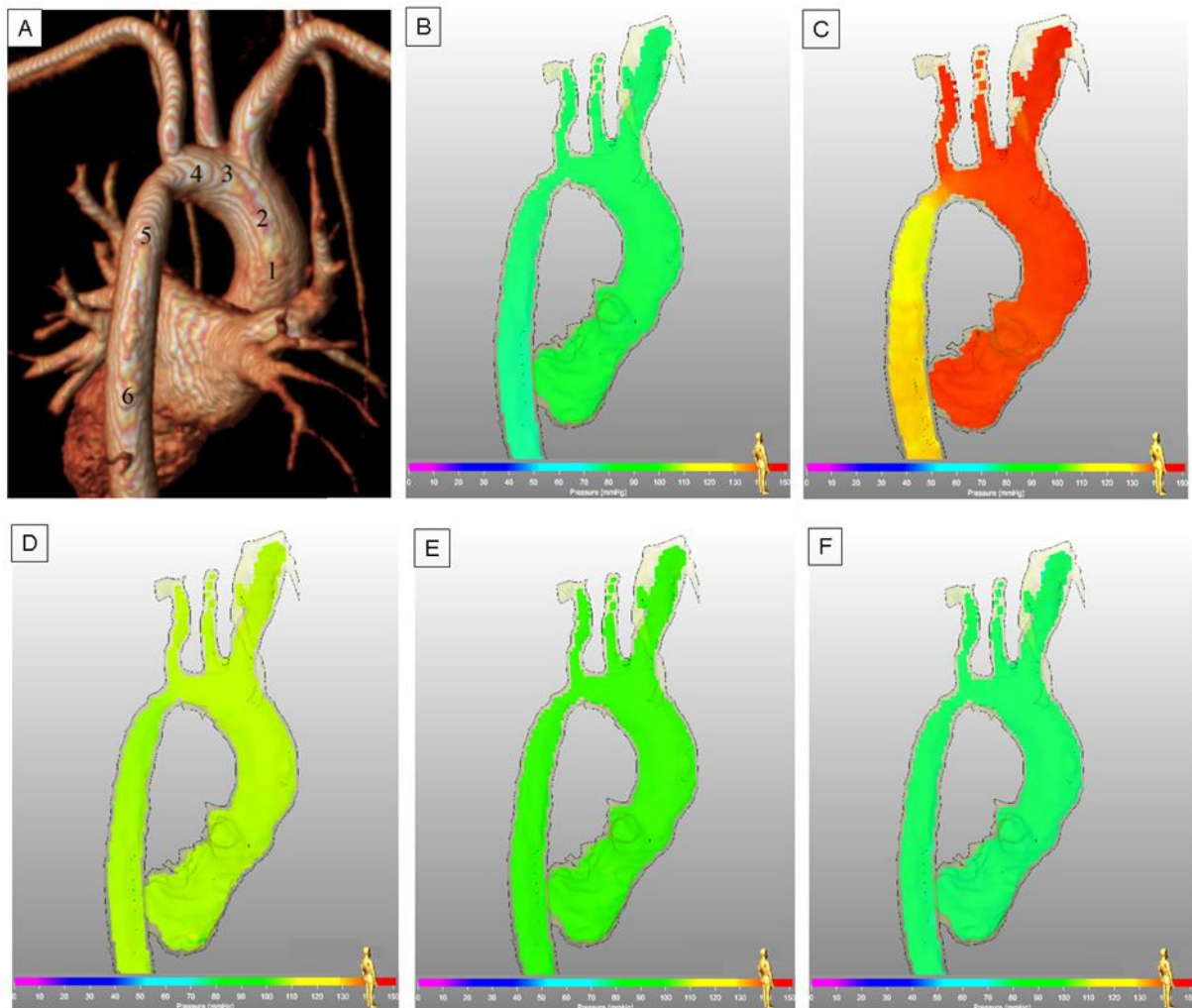


Figure 5.1 A: MR angiography of the aorta in one representative patient. The six locations for pressure measurements are shown. B to F: CMR derived 4D colour coded pressure fields calibrated with catheter, from beginning of systole to end-diastole (B: early systole, C: peak systole, D: early diastole, E: mid diastole, F: end diastole). The shown data belong to a 46 year old female patient with re-coarctation. The peak-systolic pressure gradient across the stenosis was 19 mmHg measured by catheter and 21 mmHg measured by CMR.

A finite-element-based solution for the Pressure-Poisson equation was applied to the segmented aorta for computing 4D intravascular blood pressure differences as described and verified by *Meier et al.*[103, 104] Since the Pressure-Poisson equation computation is sensitive to errors near the vessel boundaries due to high velocity gradients, a reduction of 5% on the segmented volume of the aorta was performed (to 95% of the initial segmented vessel).[104]

The blood flow velocities, measured by the 4D-VEC-MRI sequence, can be used to derive information about local pressure differences over the cardiac cycle (Figure 5.1 B to F) but not on the absolute pressure level in the blood vessel. Therefore, the pressure computation algorithm requires a calibration with a known absolute pressure profile over time at a given location in the target vessel. In the present study, the reference location was chosen to be in the ascending aorta (location 1, Figure 5.1A), Calibration was performed in two different ways:

(a) Calibration by dynamic pressures: The pressure at the reference location is considered to change over time during the cardiac cycle, and absolute dynamic pressures from catheterization are applied at the reference location. This can be considered to be the physically most realistic approach. However, it requires absolute pressure data and invasive data would be the gold standard.

(b) Calibration by static pressure: At a reference location, the pressure is considered to be constant at all-time points over the cardiac cycle. Therefore, a default zero value is applied at this reference location (in the setting in the ascending aorta at location 1) and the relative pressure differences to another predefined location (in the setting in the descending aorta at location 6) are computed for each time point. This approach is fully non-invasive, however it gives only the maximal instantaneous gradient, neglecting the shift in time of peak -systolic pressures between the ascending and descending aorta (locations 1 and 6) which is affected, among others by aortic wall compliance and the distance the pulse wave has to travel. (Figure 5.2).[105, 106]

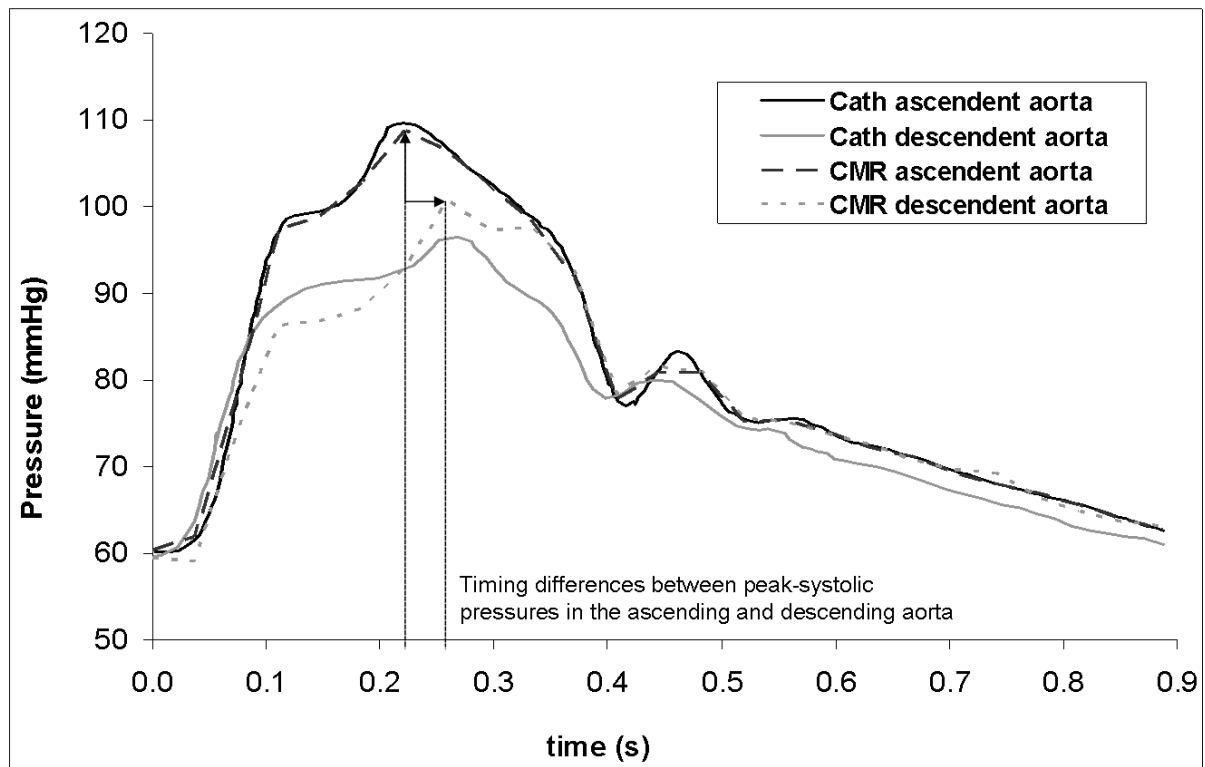


Figure 5.2 Pressure profiles of the ascending and descending aorta measured by catheterization and by CMR pressure field method with catheter calibration. The pressure profiles were obtained from a 13 year old female patient with re-coarctation in the aortic arch. The pressure profiles of the ascending aorta and the descending aorta were measured in position 2 and 6 as indicated in Figure 1, panel A. Note the timing difference in peak-systolic pressures between ascending and descending aorta (arrows)

Therefore, for the assessment of peak-systolic pressure gradients (between location 1 and 6) it was not measure the difference of pressures at the same time point but determined the differences between the “peak-to-peak” pressures at their respective time point (Figure 5.2).

### 5.1.1 Statistical analysis

Statistical testing accounted for the fact that in each patient multiple measurements were performed at six different locations along the aorta. In addition, the measurements at the position used for calibration have been excluded in order to avoid an underestimation of errors.

The agreement between catheter and CMR measurements was determined with Bland-Altman analysis for (a) systolic and diastolic pressures at the six different locations and (b) for the peak-systolic pressure gradients between locations 1 and 6 (Figure 5.1A) corresponding

respectively to ascending and descending aorta. In addition, the correlation coefficients between catheter and CMR based measures have been determined separately for the different positions (Pearson correlation coefficients).

For a common analysis of the differences measured at different positions a mixed linear model has been used.[107] The depending variable was the difference of catheter and CMR based measures at the corresponding positions. A common overall mean and a fixed effect for the position has been included as well as a random person factor. In order to respect possible dependencies of the measurements at adjacent positions, the position effect has been modelled as a repeated factor with an autoregressive correlation structure of grade 1 (AR(1)).[107]

The analyses have been carried out with SPSS version 21 (IBM Corporation, USA). Data are expressed as mean  $\pm$  standard deviation. Effects have been considered significant if  $p$  was  $< 0.05$ .

The sample size necessary to compare catheter and CMR measurements was estimated using power analysis performed with the software G\*Power 3.1.7 (Franz Faul, Kiel University, Germany). Power test was performed for the T-test (differences between two dependent means – matched pairs). As input parameters it was used: two-tails,  $\alpha=0.05$ , power= $1-\beta$  ( $\beta$  assumed as  $4*\alpha$ ), and effect size  $d=1.1$ . Effect size was calculated based on standard deviation of pressure drops measured with catheter (4.8 mmHg) and a 5 mmHg difference between two measurement techniques relevant in the clinical setting. Based on these parameters it was found that a sample size of 9 patients is necessary for this study.



## 5.2 Results

Pressures were determined by catheterization and CMR in all 13 investigated patients. The patient characteristics are given in Table 5.1.

Patient No	Sex	Age	Diagnosis	Intervention	RR Right Arm [mmHg]*	Peak-systolic gradient catheter (mmHg)†	Peak-systolic gradient CMR (mmHg)†
1	m	20	Re-CoA	Implantation of a Stent	140/60 (84)	27	27
2	f	14	Re-CoA	Implantation of a Stent	136/58 (90)	22	19
3	m	19	Re-CoA	Implantation of a Stent	146/66 (101)	15	18
4	f	23	Native CoA	Implantation of a Stent	128/62 (88)	15	10
5	f	13	Re-CoA	None	128/62 (97)	16	11
6	f	29	Re-CoA	Implantation of a Stent	140/75 (102)	16	15
7	m	52	Re-CoA	Implantation of a Stent	158/83 (115)	10	10
8	m	15	Re-CoA	None	140/55 (87)	16	15
9	m	15	Re-CoA	Implantation of a Stent	128/62 (88)	11	10
10	m	17	Re-CoA	Balloon-Dilatation	153/72 (100)	15	13
11	m	15	Native CoA	Implantation of a Stent	118/63 (74)	16	13
12	f	46	Re-CoA	Implantation of a Stent	196/88 (122)	19	21
13	f	21	Re-CoA	Implantation of a Stent	151/69 (94)	22	19

Table 5.1 Patient characteristics and pressure gradients, \* Blood pressure was measured on the right upper arm with the Riva-Rocchi (RR) method, † Gradients were measured between peak-systolic pressure values at locations 2 and 6 (Figure 5.1A), (CoA: Coarctation; Re-CoA: Re-Coarctation)

After diagnostic catheterisation, n=10 patients received the implantation of a stent, in n=1 patient a balloon angioplasty was performed, and in n=2 patients, no treatment was judged to be necessary (Table 5.1).

*Peak-systolic and diastolic pressures:* The dynamic pressure profiles obtained by catheterization and CMR were similar between the methods at all measurement positions along the aorta. Figure 5.2 shows representative pressure profiles measured in the ascending and descending aorta. The timing difference between peak-systolic pressures in the ascending

versus descending aorta is also illustrated in Figure 5.2. The correlation coefficients between both measures (catheter and CMR) varied between 0.938 and 0.973 at the different positions for the systolic pressures and between 0.956 and 0.744 for the diastolic pressures (all

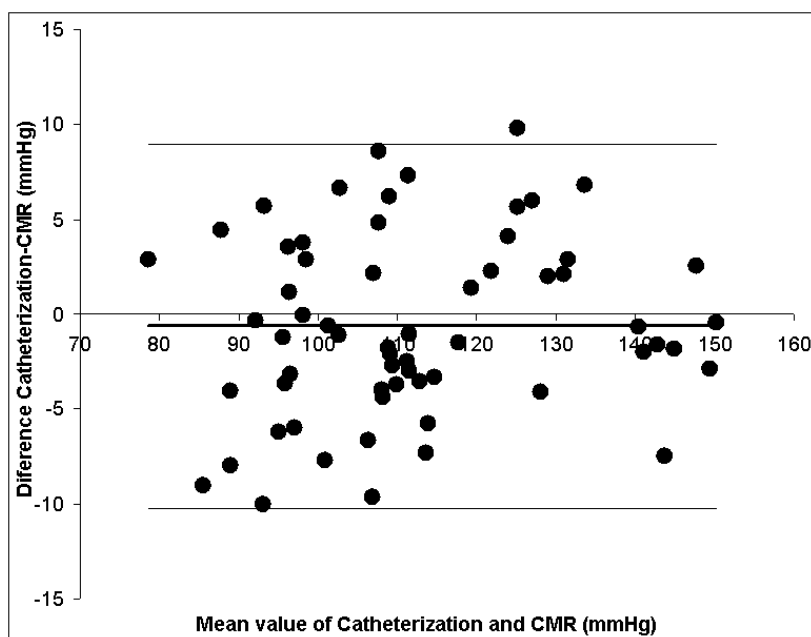


Figure 5.4 Bland-Altman plot for peak-systolic pressures measured by catheterization and CMR pressure fields in n=13 patients at different measurement locations in the ascending and descending aorta.

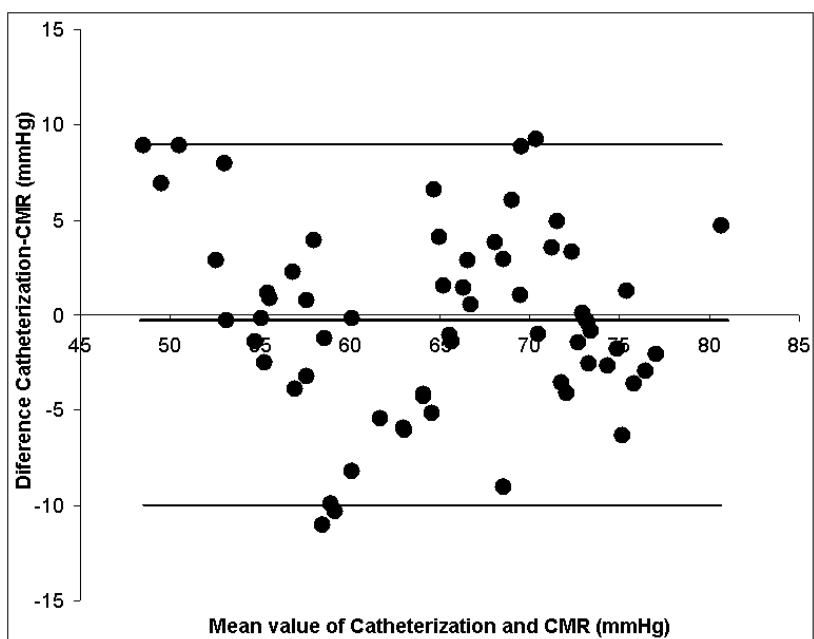


Figure 5.3 Bland-Altman plot for end-diastolic pressures measured by catheterization and CMR pressure fields in n=13 patients at different measurement locations in the ascending and descending aorta.

$p < 0.001$  in a test for independence).

There was good agreement between peak-systolic and end-diastolic pressures. For the systolic pressures, the bias (mean of differences) was  $-0.6$  mmHg and the limit of agreement (2

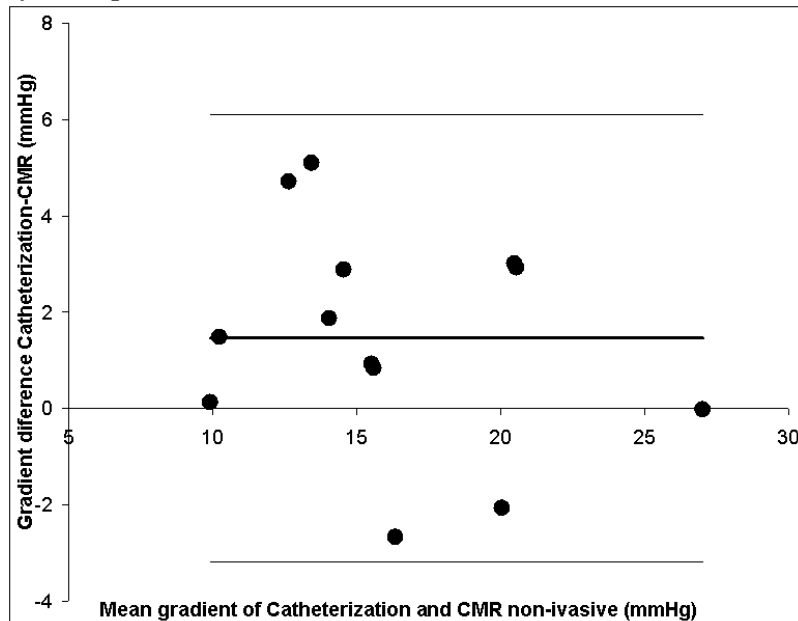


Figure 5.5 Bland-Altman plot for peak-systolic pressure gradients measured by catheterization and CMR pressure fields between two different locations in the ascending and descending aorta (location 1 and 6, Figure 1, panel A). Calibration was done with dynamic pressures obtained from catheterization (see methods section for details).

standard deviations, 2SD) was  $\pm 9.6$  mmHg (Figure 5.4). The bias suggests only slight underestimation by the CMR method with differences between the methods being not significant ( $p = 0.239$ ). For diastolic pressures, the bias

(mean of differences) was  $-0.3$  mmHg and the limit of agreement (2SD) was  $\pm 9.7$

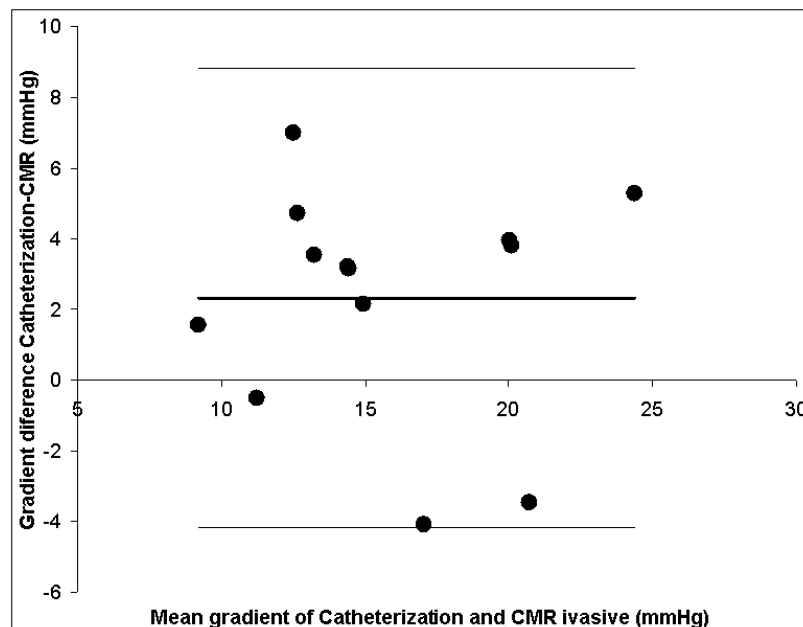


Figure 5.6 Bland-Altman plot for peak-systolic pressure gradient measured by catheterization and CMR pressure fields between two different locations in the ascending and descending aorta (location 1 and 6, Figure 1, panel A). Calibration was done with static pressures (see methods section for details).

mmHg ( $p = 0.722$ ) (Figure 5.3). The mixed model analyses showed that the difference of both measuring methods varied only slightly between the positions ( $p > 0.2$ ). Also the differences between the individual patients (person effect) had only a small effect on the variance component ( $p > 0.05$ ).

*Pressure gradients:* Bland-Altman test showed good agreement between peak-systolic pressure gradients between ascending and descending aorta measured by catheterization and the CMR pressure field method, with either calibration method (see Figure 5.6 and Figure 5.5). For calibration with dynamic catheter based pressures, the bias was 2.3 mmHg and the limit of agreement was  $\pm 6.5$  mmHg. The bias suggest only slight underestimation by the CMR method with differences between the methods being not significant ( $p=0.22$ ). For calibration by static pressure, the bias was 1.5 mmHg, and the limit of agreement was  $\pm 4.6$  mmHg. Again, the bias suggest minor underestimation by the CMR method with differences between the methods being not significant ( $p=0.45$ ).

### 5.3 Discussion

The present study provides for the first time a comparison of a CMR pressure field method with the gold standard catheterization in a group of patients with re- or native CoA. Measurements were done in a typical clinical setting in which patients had moderate pressure differences (mean= $16.9 \pm \text{SD}=4.6$  mmHg) along the aorta and thus borderline indication for catheterization and subsequent intervention. The results of this study demonstrate good agreement between the two methods.

The computation of dynamic pressure fields from CMR derived 4D flow velocities yields large promises for clinical application and science. This method allows a comprehensive yet non-invasive assessment of dynamic (time-resolved) pressures covering the entire aorta and the proximal segment of its main branches. In addition, the assessment of spatial and time resolved (4D) pressure fields can be easily combined with other VEC-MRI derived information like wall-shear stress[108] or compliance.[109] In research, such information provide the opportunity for a more differential analysis of pathophysiological processes that might be responsible for the typical sequel of CoA like arterial hypertension and associated morbidity.

For the clinical setting, 4D pressure fields are propagated for the assessment of CoA as an alternative to diagnostic catheterization. To date, in these patients precise determination of pressure gradients is one of the most common indications for diagnostic cardiac catheterization, except for cases of native severe CoA, where indication for treatment is made due to anatomical conditions.

According to current guidelines, findings of pressure measurements direct medical decision making for intervention. In the past decade, CMR evolved to an important diagnostic tool due to its superb visualization of anatomy. However, the assessment of pressure differences across the site of CoA or re-CoA using 2D-VEC-MRI and the simplified Bernoulli approach have not been convincing.[110]

Thus 4D-VEC-MRI and its derived pressure fields presenting full temporal and spatial coverage might overcome some of the former methodological limitations. Several studies investigated the accuracy of pressure field measurements in systematic phantom and initial human studies. *Bock et al.* compared gradients measured by CMR pressure field methods and Doppler echocardiography in a study of 6 patients with CoA.[111] CMR pressure differences were computed by iterative solving of Pressure-Poisson equation for each time step. The group reported good correlation between the methods but lower gradients when measured by CMR. However, it remained unclear whether these differences are due to underestimation of CMR or overestimation of Doppler echocardiography. For both methods, technical limitations that can cause under- and overestimation, respectively, are known.[110]

At the level of Doppler Echocardiography, the simplified Bernoulli's equation can cause an overestimation in the pressure calculation across a stenosis since it applies only to inviscid fluids meaning that just the convective and transient effects are considered and not the viscous loss and turbulent ones. The pressure drop in aortic coarctations is, however, associated with different terms including viscous loss, inertial effects, continuous component, and turbulent often including also momentum loss. All these effects can be estimated using 1D equations as proposed for example by *Itu et al.*[112] Because the pressure drop in aortic coarctations is mainly affected

by the momentum loss due to vortex formation behind stenosis it is well resolved by the Pressure-Poisson equation.

At the level of CMR data acquisition, spin dephasing or partial volume effects are among the prominent sources of measurement errors.[110] In order to minimize the impact of dephasing, echo times should be kept small and a reasonable trade-off between image acquisition times and spatial resolution must be defined.

At the level of CMR data processing, finite-element based method for solving the Pressure Poisson equation was applied. This finite element method was reported to limit considerably computation time and, importantly, to be less susceptible to pressure underestimation than the iterative approach of Pressure Poisson equation reported by Bock.[104, 111, 113] In addition a vessel size reduction by 5% was applied in order to avoid numerical inconsistencies close to the vessel wall typical of the Pressure-Poisson equation.[104] It was considered such minor vessel size reduction not to be critical because it was not within the scope of this study to investigate pressure conditions near the vessel, like wall shear stress.

The majority of the previous studies about CMR derived pressure fields focussed on the determination of relative pressure differences between two anatomic locations by setting pressures at the reference location to zero default values. This approach is attractive because it is easy to conduct and is fully non-invasive. However, the previous studies did not take the timing difference of peak-systolic pressures along the aorta into account.[103, 104, 111, 114] This time shift is related to the pulse wave velocities that exist in the investigated vessel segment. Pulse wave velocities vary from patient to patient and are impacted, among others, by the distance the wave has to travel and the compliance of the vessel wall.[105, 106] In CoA, the compliance of the aorta can be decreased and further affected by scars after surgery and/or stent implantation.[106] In addition, in the clinical routine, systolic pressure gradients by catheterization are typically measured as peak-to-peak gradients. For these reasons, in this study it were taken into account the timing differences of peak-systolic pressures at the different locations.

### 5.3.1 Limitations

The study was done in a cohort of 13 patients with CoA who had moderate pressure gradients with and/or without associated arterial hypertension. Such patients have borderline indications for intervention and are thus the target group for applying the proposed pressure field method as an alternative to diagnostic catheterization. In borderline conditions, pressure gradients are often determined during exercise or pharmacological stress. In this study it was not tested whether these conditions can be accurately quantified by the method presented here. In addition, the study does not provide data about measurement accuracy in severe stenosis with high pressure gradients (see Table 5.1).

The six defined anatomic positions could be slightly different between catheter and CMR based measurements

The segmentation made was not time resolved. Therefore, it does not take into account the motion of the aorta over the cardiac cycle. However, motion was accentuated at the level of the aortic annulus but less in the distal parts of the ascending aorta, the aortic arch and the descending aorta.

Absolute pressures were measured during catheterisation in sedation while CMR was performed in awaked patients. This can impact measurement accuracy because pressures and pressure gradients are affected by cardiac output.

In the present study it was not investigated interobserver or interstudy variability. However, previous work showed that 4D-VEC-MRI has relatively low variability.[99, 115]

## 6 Kinetic energy within the ventricles study

In this chapter some preliminary results of this study are shortly presented. Namely, the presentation and discussion of the main bugs detected in MevisFlow software, as well as a first KE measurement in the LV valves.

### 6.1 Methodology

Since in a previous study [5] the KE values over time were obtained for healthy subjects, this project aims to develop a procedure that gives results coherent with this previous study and then offer a first comparison between healthy volunteers and patients with congenital heart conditions in cardiac valves, by visualization and quantification of the KE in the RV and LV over a cardiac cycle.

Since this study is based on the analysis of CMR images of both LV and RV blood flow, which have natural anatomical and physiological differences (see chapter 1.1.1). The CMR images were collected (see chapter 4.1) and stored in 2 patients groups and one control group:

- LV group which include adult patients with mitral valve regurgitation (MR) either congenital or acquired. The patients were scanned before and after (up to 2 months) the intervention for reconstruction or replacement of the mitral valve. However patients with a mechanical replacement were not considered, to avoid artefacts that would be originated in the CMR. For patients of the LV group the CMR images were obtained according to the following planes: 4D flow measurement (including the 3 directions of the flow), 3CHle (3 chambers view left anatomical image), SAX (Short-axis) for patients of the LV study.
- RV group which involves adult patients between years old with pulmonary valve regurgitation (PR) and requiring an operation. This condition can either be originated by regurgitation or by a valve that requires a significantly higher ventricular pressure to open. In the RV study the patients were scanned only before an intervention for reconstruction or replacement of the pulmonary valve. For patients of the RV group the CMR images were obtained according the following planes: 4D flow measurement (including the 3 directions of the flow), 3CHri (3 chambers view right anatomical image), RVOT (Right ventricular outflow tract) and cine trans TRA-BFFE (Balanced fast field echo);
- Control group of healthy volunteers who would perform both the LV and the RV image acquisition with the respective image planes in a 1 hour CMR exam.



Before the scan, patient details were obtained: the age, gender, weight, height, body surface area (BSA), heart rate (HR) and from the scan the respective ventricular end diastolic volume (EDV), end systolic volume (ESV), stroke volume (SV) and the ejection fraction (EF). Then each set of ventricle images (containing all the different planes to ventricle analysis) per patient was stored in just one DICOM format file inside the respective patient folder.

The DICOM format files were imported to MevisFlow and Eddie Current correction was made by defining a threshold that excluded the non-moving regions outside ventricle but not inside before Calculating the PCMRA (creates the phase contrast image of the flow). In the pertinent cases a phase unwrapping was also used based on the selection of one voxel or region where a wrap was clearly visible.

Watershed 3D segmentation of the lumen was made to segment the ventricle, the atrium and the artery. Then the blood flow behavior within these cavities was analyzed.[102] Segmentation within MevisFlow can still only be made based either in the PC-MRA image or in one anatomical image plane and for just one time step. Therefore to make an analysis of a moving heart, it was necessary to consider the complete FOV of the PC-MRA image and separately make the respective moving ventricle mask in CAIPI software. The CAIPI ability of establishing clip planes in the heart valves allows a clear distinction between the ventricles and atriums or arteries. Therefore only the ventricular cavity itself is considered in the mask as can be seen in Figure 4.8.

When the segmentation of the ventricle is done for all time steps, it is possible to export the obtained mask that can be imported into MevisLab medical imaging tool.

In this project a module for MevisLab was developed that can be divided in 3 steps as can be seen in Figure 6.1A. The first consists on applying the mask segmented in CAIPI to the PC-MRA image calculated from MevisFlow. In the second one it is calculated the number of voxel within the mask and then the total volume of the mask (the volume of each voxel is known from the image acquisition). Finally, in the last step, the KE is calculated voxel by voxel as well as the total KE per time step.

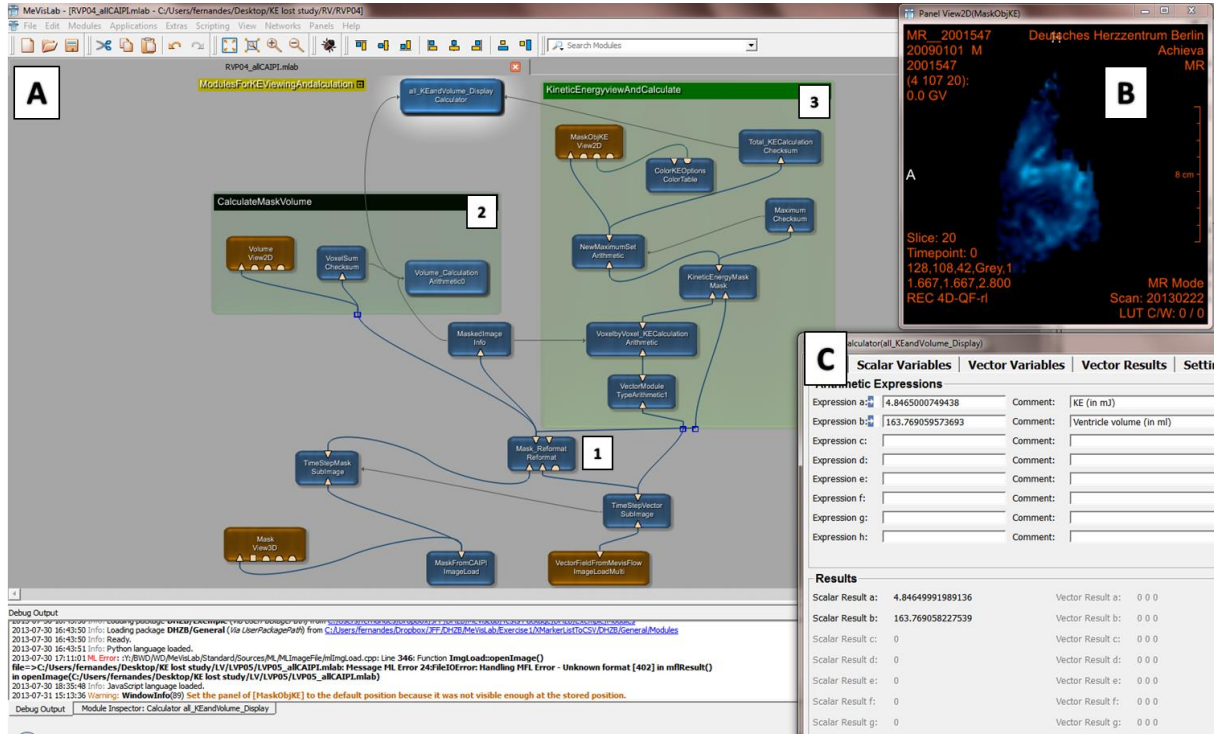


Figure 6.1 (A) MevisLab module for KE visualization and calculation. This module was developed in this project and is divided in 3 minor steps: The first (1) consists on applying the segmented mask to the PC-MRA image in the respective time step. In the second (2) the number of voxel within the mask is calculated as well as the total volume of the mask. In the third step (3) the KE is calculated voxel by voxel together with the total KE per time step. The module outputs are the 2D colour gradient KE image (B) and the total KE and blood flow volume (C) of the masked cardiovascular structure.

To fulfil this step the following equations were used. The KE should be calculated voxel by voxel following:

$$KE_{vox} = m_{vox} * v_{vox}^2$$

where  $KE_{vox}$  (in J) is the KE of one voxel,  $v_{vox}$  is the blood flow velocity (in m/s) in that voxel, and  $m_{vox}$  is the mass of the voxel. The mass of the voxel is given by:

$$m_{vox} = V_{vox} * \rho$$

where  $V_{vox}$  is the volume of each CMR voxel in  $cm^3$  and  $\rho = 1.05 \text{ g/ml}$  is the density of the blood.

These expressions allow the calculus of the KE for each voxel of a velocity vector field. When all voxels KE of a pre-established area or volume per time step ( $T$ ) are summed up it is obtained the total KE of the blood flow within that area or volume for the that time step  $T$ :

$$KE_T = \sum KE_{vox}$$

It is important to notice that, as the direction of the blood is not considered in KE calculation, the KE of blood moving in opposite directions is summed up.

The final outputs of the KE module are the 2D KE colour scale image (since the mask is 3 dimensional, is possible to change the slices of this image) of the ventricle for the given time step and the total KE and volume of the masked structure Figure 6.1 B and C. Note that calculation of the mask volume per each time step allows the obtaining of Volume and KE normalized by the volume plots.

The MevisLab results are saved as an Excel table and respective plots for KE (in mJ), volume (in ml), and KE/volume (in mJ/ml) over one cardiac cycle with 25 time steps.

All this procedures will be used in a future more complete project. In the following 2 sub-chapters are only presented the first results according to this procedure.

## 6.2 Results

In this section it will be presented the first KE results (curves and images) obtained from the methodology previously presented for both LV and RV.

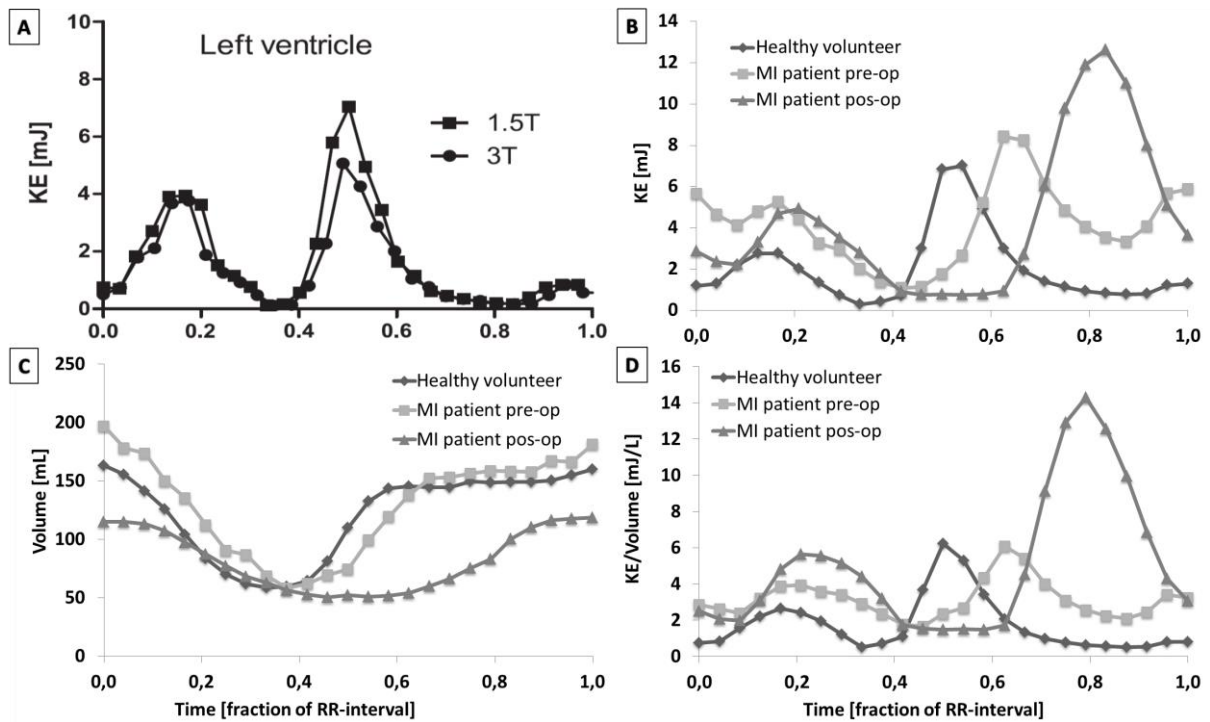


Figure 6.2 A: Blood flow kinetic energy (KE) curves (in mJ) over the cardiac cycle (time normalized) within a healthy subject left ventricle (LV) obtained by Carlsson et al. in a 1.5 and a 3 Tesla CMR scanners.[5] All the remaining curves (B to D) compare a healthy subject and a patient with mitral insufficiency before and after an intervention to the respective valve. B: KE curves (in mJ) over the cardiac cycle (time normalized); C: Volume curves (in mL) over the cardiac cycle (time normalized); D: Volume normalized KE curves over the cardiac cycle (time normalized). These are the first results obtained from the presented methodology applied to LV. These are also the first ever results considering KE within a diseased LV.

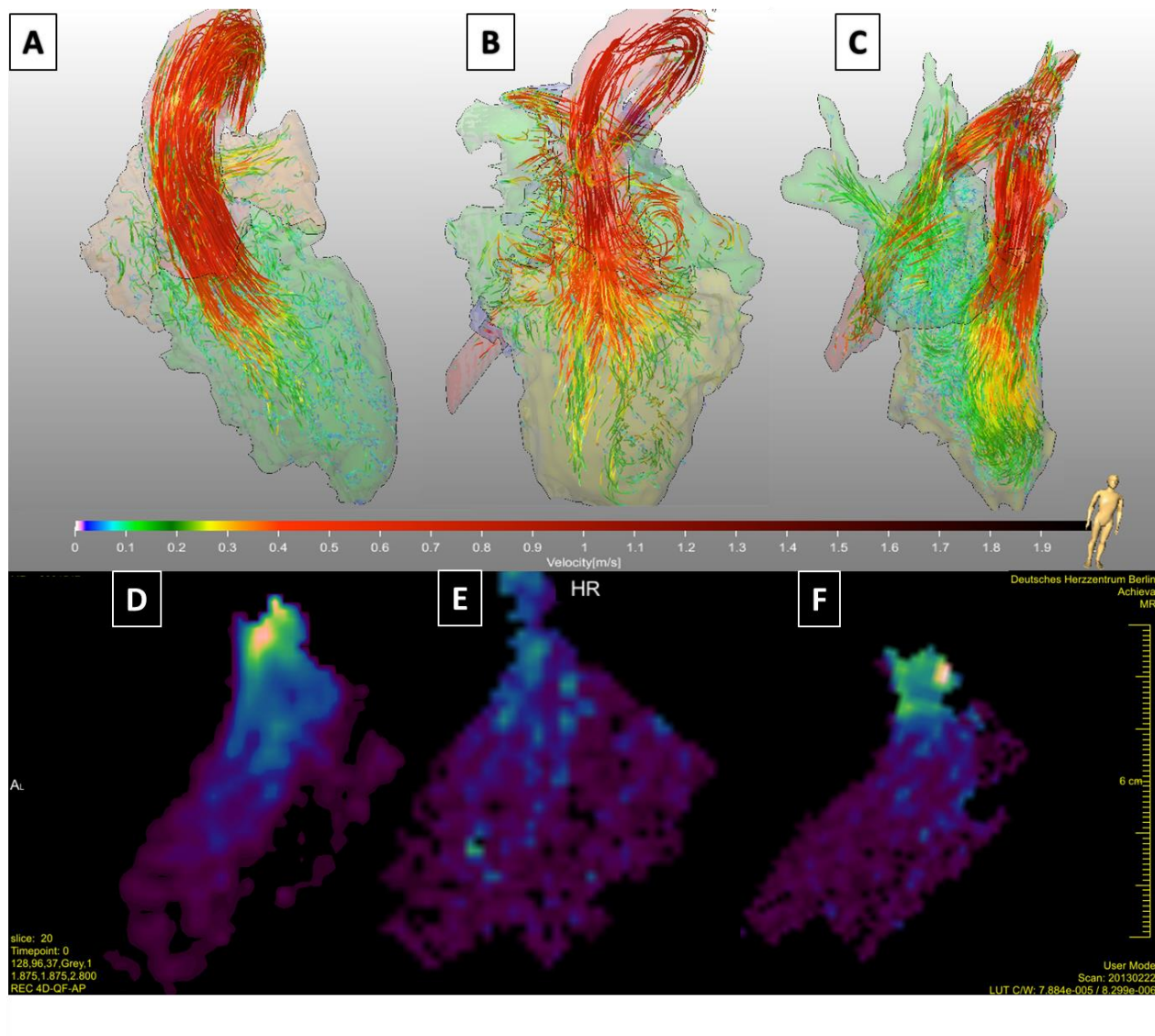


Figure 6.3 Peak left ventricle (LV) systole (moment in which more blood is being ejected from the ventricle) images of 3D blood flow tracing with velocity colour scale (up) and 2D kinetic energy (KE) colour gradient in the long axis longitudinal view (down). The blood flow tracing images include a static segmentation of the LV, left atrium (LA) and aorta artery (Ao), whereas the KE include only the LV. The images on the left (A and D) were obtained from a healthy subject. The middle images (B and E) were obtained from a patient with mitral valve insufficiency before intervention. The images on the right (C and F) were also from the same patient, but after intervention. (AL: left-anterior direction according to the anatomical position, HR: right-head direction according to the anatomical position of descending aorta)



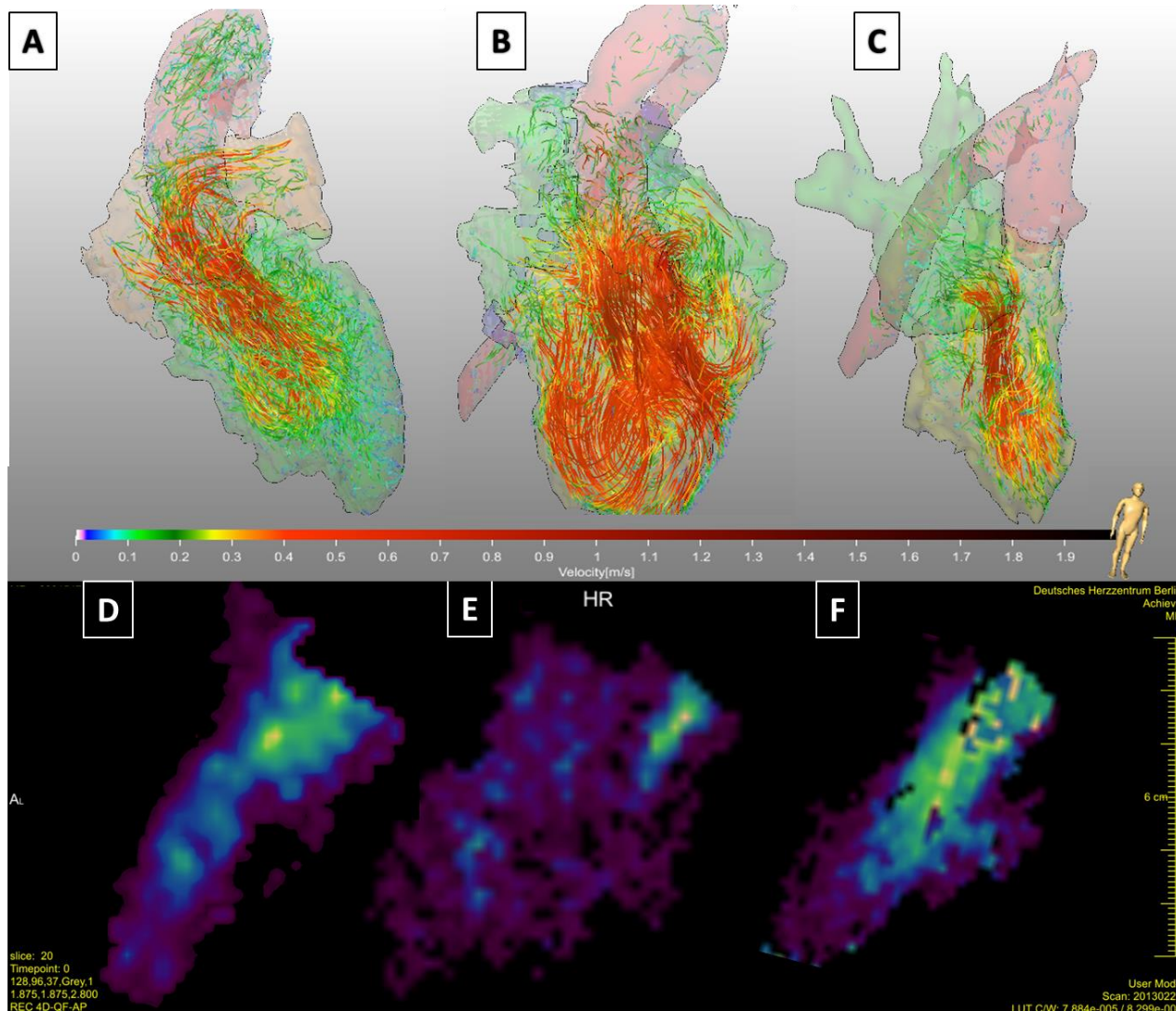


Figure 6.4 Peak left ventricle (LV) diastole (moment in which less blood is being ejected from the ventricle) images of 3D blood flow tracing with velocity colour scale (up) and 2D kinetic energy (KE) colour gradient in the long axis longitudinal view (down). The blood flow tracing images include a static segmentation of the LV, left atrium (LA) and aorta artery (Ao), whereas the KE include only the LV. The left images (A and D) were obtained from a healthy subject. The middle images (B and E) were obtained from a patient with mitral valve insufficiency before intervention. The right images (C and F) were also from the same patient, but after intervention. (AL: left-anterior direction according the anatomical position, HR: right-head direction according the anatomical position descending aorta)

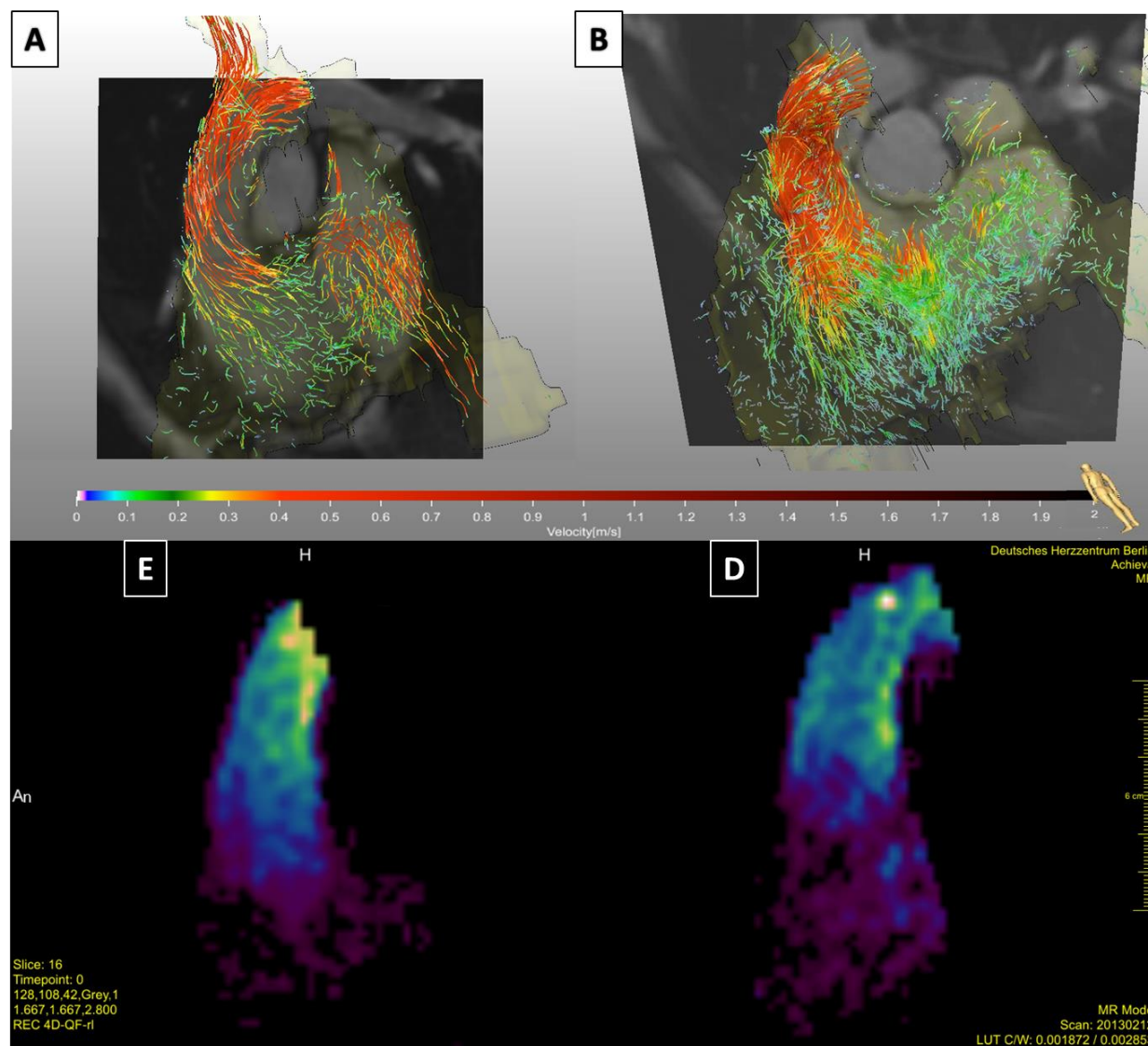


Figure 6.5 Peak right ventricle (RV) systole (moment in which more blood is being ejected from the ventricle) images of 3D blood flow tracing with velocity colour scale (up) and 2D kinetic energy (KE) colour gradient in the long axis longitudinal view (down). The blood flow tracing images include a static segmentation of the RV, right atrium (RA) and pulmonary artery (PA), whereas the KE include only the RV. The left images (A and C) were obtained from a healthy subject. The right images (B and D) were obtained from a patient with pulmonary valve insufficiency before intervention. (An: anterior direction according to the anatomical position, H: head direction according to the anatomical position descending aorta)

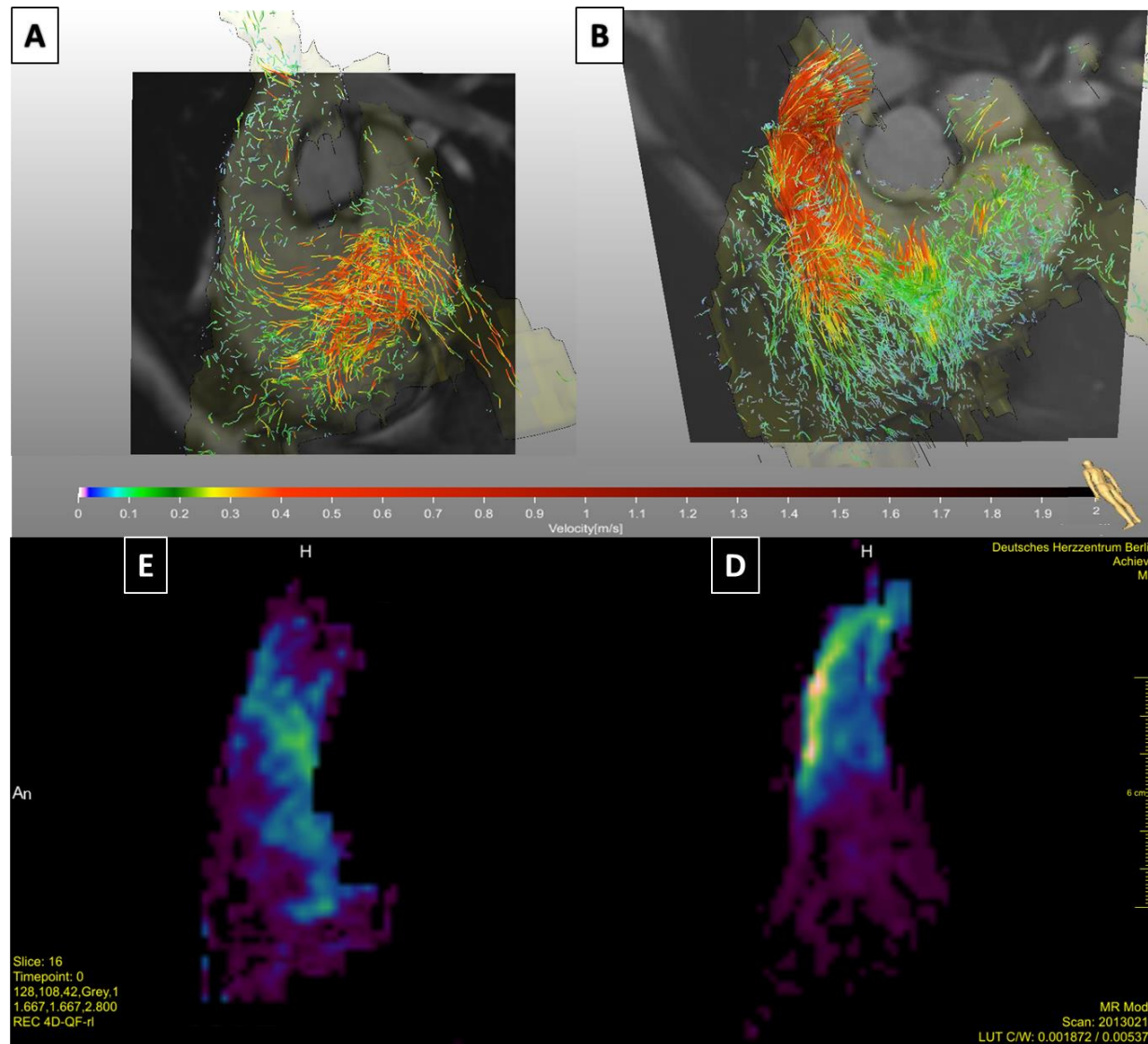


Figure 6.6 Peak right ventricle (RV) diastole (moment in which more blood is entering in the ventricle) images of 3D blood flow tracing with velocity colour scale (up) and 2D kinetic energy (KE) colour gradient in the long axis longitudinal view (down). The blood flow tracing images include a static segmentation of the RV, right atrium (RA) and pulmonary artery (PA), whereas the KE include only the RV. The left images (A and C) were obtained from a healthy subject. The right images (B and D) were obtained from a patient with pulmonary valve insufficiency before intervention. (An: anterior direction according to the anatomical position, H: head direction according to the anatomical position descending aorta)

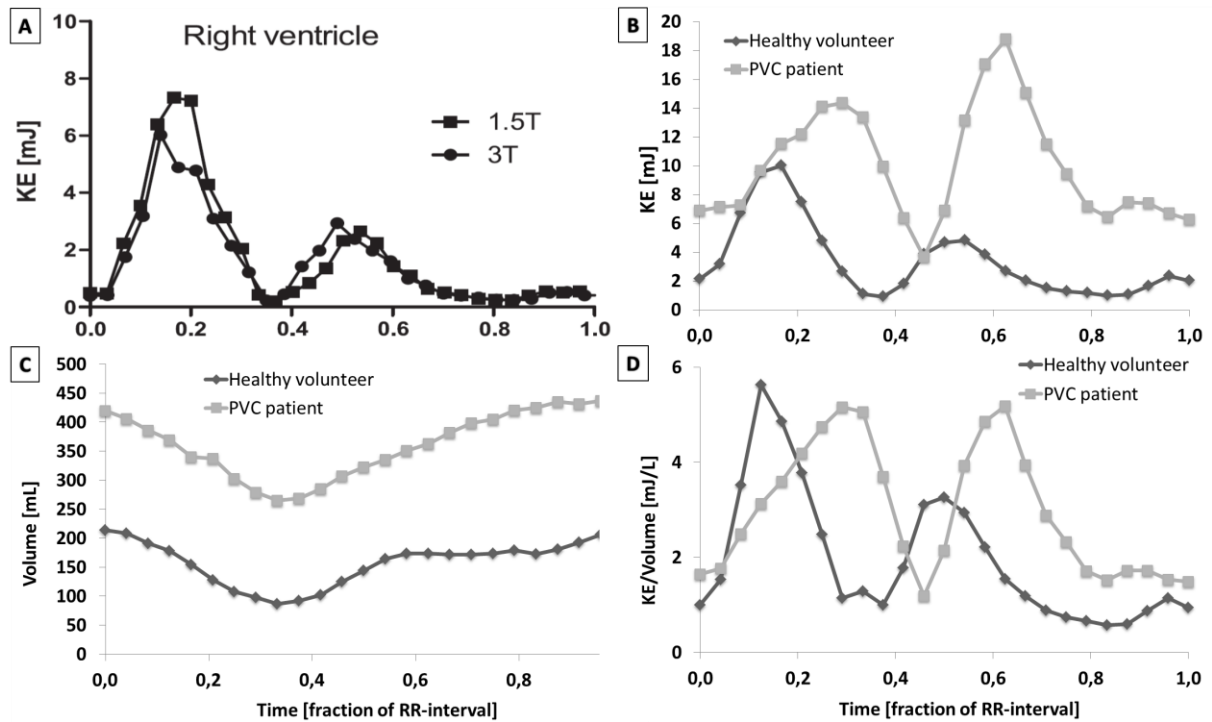


Figure 6.7 A: Blood flow kinetic energy (KE) curves (in mJ) over the cardiac cycle (time normalized) within a healthy subject right ventricle (RV) obtained by Carlsson et al. in a 1.5 and a 3 Tesla CMR scanner. (Carlsson et al). All the remaining curves (B to D) compare a healthy subject and a patient with pulmonary insufficiency before intervention to the respective valve. B: KE curves (in mJ) over the cardiac cycle (time normalized); C: Volume curves (in mL) over the cardiac cycle (time normalized); D: Volume normalized KE curves over the cardiac cycle (time normalized). These are the first results obtained from the presented methodology applied to RV. These are also the first ever results considering KE within a diseased RV.



### 6.3 Discussion

The present study provides a first comparison between blood flow kinetic energies within healthy and non-healthy LV and RV. Since the aim was to study the effect that valves with conditions and regurgitation have in the blood flow and KE, both the non-healthy LV and RV included had congenital heart valve diseases. In the formation of a LV group, it was considered that the mitral valve has too high maximum velocities compared to the low speed blood flow that is aimed to study within the ventricle. If a high VENC would be implemented there would be less sensitivity to low speeds and therefore not so accurate KE values in diastole. Thus it was chosen a low VENC of 150cm/s. In the future, with the development of postprocessing image techniques the accuracy of measurements in vessels where there is relatively big changes in blood velocity over a cardiac cycle tends to increase. The RV group is based on the pulmonary valve regurgitation patients (PR), since there are several datasets of patients with pulmonary regurgitation. Also the fact that the tricuspid valve regurgitation is hard to identify in the CMR images since it is very close to the pulmonary valve.[116] Note that, while in the LV, the patients were scanned before and within 6 month after the exam, in the RV group only the pre-interventional exam is included. It is not included post-interventional pulmonary patients because they usually come for routine CMR as follow-up examinations where a 4D flow acquisition is not made.

Other issue regards the patients that have a mechanic valve replacement in the LV and in the RV. Since the mechanical replacement is usually made with materials that create artefacts that reduce the quality of image and as a consequence, reduce also the accuracy of the blood flow velocities and KE measurements.[117]

In order to store the images DICOM format files were used since this is the only image format that can be imported into MevisFlow. Therefore it is the only way to calculate the PC-MRA images and have the blood flow velocities values per voxel per cardiac cycle. It is also accepted by CAIPI.

Since the MevisFlow segmentation can only be based on just one time step either in PC-MRA image or in one anatomical image plan, the resulting segmentation would always be inaccurate. This is due to the moving ventricle during each heart cycle, and thus the volume of moving blood within the ventricle is also always changing. Therefore in MevisFlow segmentation it is only possible to segment a single PC-MRA image or to consider one anatomical image plane, for one time step. This is the reason for combining the complete FOV of the PC-MRA image and the respective moving ventricle mask segmented in CAIPI software. In CAIPI it is possible to

make a watershed 3D segmentation based in 4 different planes at the same time for all the time steps of the cardiac cycle.

Another advantage of using the CAIPI software is related with the cardiac valves. When the valves are open it is almost impossible to do an automatic segmentation based on the contrast in order to distinguish between what is ventricle and what is atrium or artery in the CMR image. Therefore CAIPI software valve clip planes are very useful. This procedure avoids the problem of having the same contrast intensity on both sides of the valve, and therefore, it makes possible to include the valve region on the segmentation. By setting a valve circular area, this problem is solved and only the ventricle lumen is included in the segmentation. The fact that is also possible to manage this planes in 4 different CMR image plane sets, improves the accuracy of its position.

Finally the mask of a moving ventricle originated by CAIPI has the same world matrix and time steps as the PC-MRA image. Thus is possible to apply it to the PC-MRA FOV that contains the velocities per voxel in a MevisLab module.

In the calculation of the KE it is important to notice that, as the direction of the blood is not considered in KE calculation, the KE of blood moving in opposite directions is summed up. This can possibly means that the ventricular KE is related ventricular turbulence which is known to be higher in ventricles with regurgitation valves.

The plots of the KE energy over time are results of most important for this study since they take both velocities and volume, which are the variables that influence the final KE value. The obtained KE plots normalized over volume are important since that allow a direct comparison between the blood flow KE profiles of ventricles with different volumes. Note that each heart has its own different temporal periods for the different cardiac cycle phases, and therefore is natural that peak diastole and peak systole normalized time step vary from subject to subject. Nevertheless, the peak systolic and peak diastole can easily distinguished for each patient in the KE and KE over volume graphs (see Figure 6.2 and Figure 6.7) Note that the CMR starts record the CINE images in the beginning of the systole and the post-processing resulting curves are a consequence of it since the first period considered in the curve corresponds to the systole and the second period corresponds to diastole. Depending on the heart cycle recorded the diastole can start from 35% to 60% of the total heart cycle time and is therefore related with the heart cycle of each subject exam.

As this study was a first approach to the procedures used, few subjects were included. The biggest concern was to obtain results regarding healthy volunteers coherent with previous studies of *Carlsson et al*, what was verified (see Figure 6.3, Figure 6.4, Figure 6.5 and Figure 6.6), and be able to make an interpretation of the first results of ventricles with conditions.[5]

The first step on the discussion of the results is to compare the results obtained by *Carlsson et al*. (Figure 6.2A and Figure 6.7A) with the results obtained with 1.5T scan for the

healthy volunteer according the method used in this study (see chapter 6.1 Methodology) for both ventricles (Figure 6.2B and Figure 6.7B). In the LV case, it is possible to verify that the curve profile is essentially the same, with just a 1mJ less in peak systole KE and with the same peak diastole KE (7mJ). Also in the RV case it is possible to notice that the KE curve of a healthy volunteer as a similar profile as the mean of patients obtained by *Carlsson et al.*, but with a slightly higher KE of 1mJ due to residual blood (blood that stays within the heart during the whole cardiac cycle). This is due to the high volume of the healthy RV considered. Therefore is natural, that in the moments where the blood is circulating faster, correspondent to the diastolic and systolic peaks, the KE were even higher reaching 2mJ more than in *Carlsson et al.* results. This fact supports the hypothesis that the methodology used to calculate the ventricle KE is coherent whit the previous study of ventricular KE.[5] Although initial results suggest that this first objective was achieved, a higher number of healthy volunteers should be included in a future study to make a more certain comparison.

In the analysis of the LV KE profile of the patient before and after operation several interesting aspects are visible. Firstly it can be seen that this patient needs a relatively long systole compared with the healthy volunteer, and that this period is even longer after the mitral valve intervention. This is very interesting since it seems to indicate that when the atrio-ventricular valve is replaced in the LV, the blood needs more time to be transferred from the atrium to the ventricle (BIBLIO). This could also be an interesting point to start a new study on how valve replacement or reconstruction affect the cardiac cycle. Secondly, and more importantly for the present study, it is verified that a patient with a mitral valve insufficiency has significantly higher (2 times more) LV KE in systole that a healthy LV. That can be explained by the fact that the ventricle pumps blood to aorta but also back to the atrium and therefore the flow is significantly more turbulent, having higher absolute velocity and thus higher KE (see Figure 6.3B and E). Also the diastolic KE peak was 1,5 mJ higher in the pre operation LV than in the Healthy LV, which may be due to the higher volume that the diseased ventricle has (see Figure 6.2 C). However the most interesting result is the post-operation LV KE curve, since it shows that after the valve was reconstructed instead of reducing, the ventricle KE was maintained in systole and even increased in diastole. Since the new valve needs higher atrial blood pressure to open, it takes more time to open and when the blood enters in the ventricle it does so with much higher velocity (see Figure 6.4 C and F) and thus KE also increases. This aspect is even more visible when KE was normalized in relation to the volume, since the post-operation LV has less blood volume without any regurgitation (BIBLIO) (see Figure 6.2 D). In fact removing the volume variable, it can be see that the LV with the reconstructed valve has a KE 8mJ/L higher than it had before intervention and compared to a healthy ventricle (6mJ/L). In this the systolic peak is naturally higher than the pre-operation value since the ventricle blood flow is lower, but it pumps the blood with the same

geometry as before and probably with roughly the same strength, which is translated into very high velocities and high stroke volume .

In the RV KE analysis, it can be seen that the pulmonary valve insufficiency is translated in a ventricle with a big volume (see Figure 6.7 C), more blood being ejected in systole than in a healthy ventricle in the physiological process of compensating for pulmonary regurgitation by sending more blood to the pulmonary artery. And it can also be observed that there is a very high KE in late diastole and early systole (see Figure 6.7 B), correspondent to the residual blood which is due to the very big volume of the RV. Together, all these facts, result in a considerably higher systolic peak (14mJ) than in the healthy ventricle (10mJ). However the major change in the curve profile occurs in the diastole whose peak is higher than the diastolic one, the opposite of the healthy RV. This is due to the blood that returns to the ventricle by the pulmonary artery plus the blood that arrives to the heart in non-pathologically conditions by the right atrium. This amount of moving blood increases the KE energy meaning that even when it is normalized in order to the volume, the systolic peaks are similar, but there is a 2mJ/L difference between the diseased ventricle (5mJ/L) and the healthy one (3mJ/L).

Also the fact that bigger ventricles have more blood and therefore are more likely to have relatively higher KE has been proven before and was observed also in this study (Figure 6.1C and Figure 6.7C). It was also observed that KE tends to be higher in places where there is more turbulence and non-linear blood flow paths like the heart valves. (see Figure 6.3, Figure 6.4, Figure 6.5 and Figure 6.6)

Once more, in both RV and LV analysis more samples will be needed in order to confirm these results and discuss in more detail the ventricular KE physiological process. Nevertheless, the results look promising and maybe in a near future this new measurement of evaluating the heart performance may be available for clinical practice.

## 7 Conclusion

This work is an example of joining knowledge from different fields, performed by a person whose formation is essentially physics working in a group of cardiovascular doctors formed in medicine and biology. By working together there is a better mutual understanding of each other's necessities and objectives, which in the end merge. Therefore it is natural that there was a slightly different approach in this project from the pure biomedical research ones. Nevertheless, this dissertation shows that postprocessing of the images from a normal imaging scanner, in this case CMR, can improve the quality of the exams by supplying more diagnosing measurements or supplying the same but non-invasively. Another positive aspect is the fact that as long as the studies return valid results and understanding and the softwares get clinical approval, these measurements can become easily available for every CMR diagnosis without the need for setting up a new machine or change completely the software. The non-invasive measurement of pressure gradients can in a near future replace the diagnostic catheterization, which has the natural risks of being an invasive technique. This means that only in cases where the stent implementation or other intervention is needed will it be necessary to perform catheterization. Although the study of ventricular blood flow KE in diseased patients needs further investigation, the first results seem to indicate that such measurements can be very useful for the better understanding of ventricular function in healthy but especially non-healthy patients, and has the potential to be of considerable value in future valve replacement interventions.

In conclusion, these new approaches to the analysis of cardiovascular images allow a better comprehension of the cardiovascular system, and in the future can lead to personalised therapy planning of cardiovascular pathologies, increasing their success rate and therefore reduce the major pathological cause of deaths in the human population.[8] However, before real clinical diagnosing and predictive value of flow measurements, there is still the need for further investigation, especially with larger trials and studies before and after interventions, therapies or during a conditions progression.

As an outcome for this work, a scientific paper is currently under consideration for publication in the International Journal of Cardiology (Impact factor of 5.509 [118]) based on the pressure gradient across an aortic coarctation study with the title: "Pressure fields by flow-sensitive four-dimensional velocity-encoded magnetic resonance imaging in patients with aortic coarctation" and co-authored by: Eugénie Riesenkampff, MD, **Joao Filipe Fernandes**, Sebastian Meier, Leonid Goubergrits, Siegfried Kropf, Stephan Schubert, MD, Felix Berger, MD, Anja Henneumuth, Titus Kuehne, MD.

## 8 Bibliography

1. *Post BMV echocardiogram*. 2010; Available from: <http://cardiophile.org/wp-content/uploads/2010/01/MS-PLAX-Colour-Doppler.jpg>.
2. Clinic, C. *Aorta Anatomy*. [cited 2013; Available from: <http://my.clevelandclinic.org/heart/heart-blood-vessels/aorta.aspx>
3. Frederic H. Martini, P.D., P.D. Judi L. Nath, and M.S. Edwin F. Bartholomew, *Fundamentals of Anatomy and Physiology*. 9th ed 2012: Benjamim, Cummings.
4. Donna D. Ignatavicius, M.L.W., *Medical-Surgical Nursing: Critical Thinking for Collaborative Care*. 2nd ed 2002.
5. Carlsson, M., et al., *Quantification of left and right ventricular kinetic energy using four-dimensional intracardiac magnetic resonance imaging flow measurements*. American Journal of Physiology-Heart and Circulatory Physiology, 2012. **302**(4): p. H893-H900.
6. Markl, M., P.J. Kilner, and T. Ebbers, *Comprehensive 4D velocity mapping of the heart and great vessels by cardiovascular magnetic resonance*. Journal of Cardiovascular Magnetic Resonance, 2011. **13**(1): p. 1-22.
7. WHO. *Cardiovascular diseases (CVDs)*. 21-Dec-2012]; Available from: <http://www.who.int/mediacentre/factsheets/fs317/en/index.html>.
8. Baumgartner, H., *Geriatric congenital heart disease: a new challenge in the care of adults with congenital heart disease?* European Heart Journal, 2013.
9. Warnes, C.A., et al., *ACC/AHA 2008 Guidelines for the Management of Adults With Congenital Heart Disease: A Report of the American College of Cardiology/American Heart Association Task Force on Practice Guidelines (Writing Committee to Develop Guidelines on the Management of Adults With Congenital Heart Disease): Developed in Collaboration With the American Society of Echocardiography, Heart Rhythm Society, International Society for Adult Congenital Heart Disease, Society for Cardiovascular Angiography and Interventions, and Society of Thoracic Surgeons*. Circulation, 2008. **118**(23): p. e714-e833.
10. Cassidy, S.C., et al., *Complications of pediatric cardiac catheterization: A 3-year study*. Journal of the American College of Cardiology, 1992. **19**(6): p. 1285-1293.
11. Eriksson, J., et al., *Semi-automatic quantification of 4D left ventricular blood flow*. J Cardiovasc Magn Reson, 2010. **12**(9).
12. Gray, H., *Anatomy of the human body*. 20th ed. ed 1918.
13. J. Enderle, S.M.B., and J. Bronzino, *Introduction to Biomedical Engineering*, 2005, Academic Press.
14. Hager, A., et al., *Coarctation Long-term Assessment (COALA): Significance of arterial hypertension in a cohort of 404 patients up to 27 years after surgical repair of isolated coarctation of the aorta, even in the absence of restenosis and prosthetic material*. The Journal of thoracic and cardiovascular surgery, 2007. **134**(3): p. 738-745.e2.
15. Feltes, T.F., et al., *Indications for Cardiac Catheterization and Intervention in Pediatric Cardiac Disease: A Scientific Statement From the American Heart Association*. Circulation, 2011. **123**(22): p. 2607-2652.
16. Golden, A.B. and W.E. Hellenbrand, *Coarctation of the aorta: Stenting in children and adults*. Catheterization and Cardiovascular Interventions, 2007. **69**(2): p. 289-299.
17. Forrester JS, G.W., Diamond G, McHugh T, Chonette DW, Swan HJ., *Thermodilution cardiac output determination with a single flow-directed catheter*. Am Heart J. 1972. **83**(3): p. 306-11.
18. Vale, P.R., et al., *Randomized, Single-Blind, Placebo-Controlled Pilot Study of Catheter-Based Myocardial Gene Transfer for Therapeutic Angiogenesis Using Left Ventricular Electromechanical Mapping in Patients With Chronic Myocardial Ischemia*. Circulation, 2001. **103**(17): p. 2138-2143.
19. Smith, D.C., G.S. Grable, and D.J. Shipp, *Safe and effective catheter angiography through prosthetic vascular grafts*. Radiology, 1981. **138**(2): p. 487-488.

20. Dick, E.A., et al., *Catheter angiography and angioplasty in patients with scleroderma*. British Journal of Radiology, 2001. **74**(888): p. 1091-1096.
21. Yock, P.G., *Method and apparatus for intravascular ultrasonography*, 1999, Cardiovascular Imaging System, Inc.
22. Godart, F., *Intravascular stenting for the treatment of coarctation of the aorta in adolescent and adult patients*. Archives of Cardiovascular Diseases, 2011. **104**(12): p. 627-635.
23. B.Lee, L., *Biography: History of developments in imaging techniques: Egas Moniz and angiography*. Seminars in Pediatric Infectious Diseases, 2003. **14**(2): p. 173-181.
24. Brentnall, P., *Equipment for Fluoroscopy and Angiography* 2012: University of the Lst of England.
25. Members, C., et al., *ACC/AHA Guidelines for Coronary Angiography: Executive Summary and Recommendations: A Report of the American College of Cardiology/American Heart Association Task Force on Practice Guidelines (Committee on Coronary Angiography) Developed in collaboration with the Society for Cardiac Angiography and Interventions*. Circulation, 1999. **99**(17): p. 2345-2357.
26. Prevrhal, S., et al., *CT Angiographic Measurement of Vascular Blood Flow Velocity by Using Projection Data*. Radiology, 2011. **261**(3): p. 923-929.
27. Min, J.K., et al., *Usefulness of Noninvasive Fractional Flow Reserve Computed from Coronary Computed Tomographic Angiograms for Intermediate Stenoses Confirmed by Quantitative Coronary Angiography*. The American journal of cardiology, 2012. **110**(7): p. 971-976.
28. Bamberg, F., et al., *Accuracy of Dynamic Computed Tomography Adenosine Stress Myocardial Perfusion Imaging in Estimating Myocardial Blood Flow at Various Degrees of Coronary Artery Stenosis Using a Porcine Animal Model*. Investigative Radiology, 2012. **47**(1): p. 71-77 10.1097/RLI.0b013e31823fd42b.
29. Park, K.W., et al., *Regional cerebral blood flow differences in patients with mild cognitive impairment between those who did and did not develop Alzheimer's disease*. Psychiatry Research: Neuroimaging, 2012. **203**(2): p. 201-206.
30. Headings, N.L.o.M.-M.S. *Myocardial Perfusion Imaging*. Available from: [http://www.nlm.nih.gov/cgi/mesh/2011/MB\\_cgi?mode=&term=Myocardial+Perfusion+Imaging](http://www.nlm.nih.gov/cgi/mesh/2011/MB_cgi?mode=&term=Myocardial+Perfusion+Imaging).
31. Di Carli, M.F. and V.L. Murthy, *Cardiac PET/CT for the evaluation of known or suspected coronary artery disease*. Radiographics, 2011. **31**(5): p. 1239-1254.
32. Einstein, A.J., et al., *Radiation dose to patients from cardiac diagnostic imaging*. Circulation, 2007. **116**(11): p. 1290-1305.
33. Einstein, A.J., M.J. Henzlova, and S. Rajagopalan, *Estimating risk of cancer associated with radiation exposure from 64-slice computed tomography coronary angiography*. JAMA: the journal of the American Medical Association, 2007. **298**(3): p. 317-323.
34. Brenner, D.J. and E.J. Hall, *Computed tomography—an increasing source of radiation exposure*. New England Journal of Medicine, 2007. **357**(22): p. 2277-2284.
35. Correale, M., et al., *Controversies in echocardiography: 2D vs 3D vs 4D*. Minerva cardioangiologica, 2009. **57**(4): p. 443.
36. Bushberg J.T., S.J.A., et al. , *The essential physics of medical imaging*. 2nd ed ed2002, Philadelphia.
37. Agarwala, B. and A. Ghosh, *2-Dimensional and Color-Flow Doppler Imaging of Coronary Anomalies*. Texas Heart Institute Journal, 2010. **37**(2): p. 250.
38. Nagueh, S.F., et al., *Tissue Doppler imaging consistently detects myocardial abnormalities in patients with hypertrophic cardiomyopathy and provides a novel means for an early diagnosis before and independently of hypertrophy*. Circulation, 2001. **104**(2): p. 128-130.
39. Fukuda, K., et al., *Regional left ventricular wall motion abnormalities in myocardial infarction and mitral annular descent velocities studied with pulsed tissue Doppler imaging*. Journal of the American Society of Echocardiography, 1998. **11**(9): p. 841-848.
40. Bolognesi, R., et al., *Detection of early abnormalities of left ventricular function by hemodynamic, echo-tissue Doppler imaging, and mitral Doppler flow techniques in patients*

- with coronary artery disease and normal ejection fraction. *Journal of the American Society of Echocardiography*, 2001. **14**(8): p. 764-772.
41. Ghorbani, A., F. Ashtari, and F. Fatehi, *The assessment value of transcranial Doppler sonography versus magnetic resonance angiography in vertebrobasilar stroke*. *Journal of research in medical sciences: the official journal of Isfahan University of Medical Sciences*, 2010. **15**(3): p. 133.
  42. Ommen, S., et al., *Clinical utility of Doppler echocardiography and tissue Doppler imaging in the estimation of left ventricular filling pressures a comparative simultaneous Doppler-catheterization study*. *Circulation*, 2000. **102**(15): p. 1788-1794.
  43. Sohn, D.-W., et al., *Assessment of mitral annulus velocity by Doppler tissue imaging in the evaluation of left ventricular diastolic function*. *Journal of the American College of Cardiology*, 1997. **30**(2): p. 474-480.
  44. Seifert, B.L., et al., *Accuracy of Doppler methods for estimating peak-to-peak and peak instantaneous gradients across coarctation of the aorta: An In vitro study*. *Journal of the American Society of Echocardiography*, 1999. **12**(9): p. 744-753.
  45. Saraste, A. and J. Knuuti, *Cardiac PET, CT, and MR: what are the advantages of hybrid imaging?* *Current cardiology reports*, 2012. **14**(1): p. 24-31.
  46. Kaufmann, P.A., *Cardiac hybrid imaging: state-of-the-art*. *Annals of nuclear medicine*, 2009. **23**(4): p. 325-331.
  47. Marinelli, M., et al., *Hybrid image visualization tool for 3D integration of CT coronary anatomy and quantitative myocardial perfusion PET*. *International journal of computer assisted radiology and surgery*, 2013: p. 1-12.
  48. Uren, N.G., et al., *Relation between myocardial blood flow and the severity of coronary-artery stenosis*. *New England Journal of Medicine*, 1994. **330**(25): p. 1782-1788.
  49. Vargas, M.-I., et al., *Approaches for the optimization of MR protocols in clinical hybrid PET/MRI studies*. *Magnetic Resonance Materials in Physics, Biology and Medicine*, 2013: p. 1-13.
  50. Stegger, L., et al., *Simultaneous PET/MR imaging of the brain: feasibility of cerebral blood flow measurements with FAIR-TrueFISP arterial spin labeling MRI*. *Acta Radiologica*, 2012. **53**(9): p. 1066-1072.
  51. Manka, R., et al., *Hybrid cardiac magnetic resonance/computed tomographic imaging: first fusion of three-dimensional magnetic resonance perfusion and low-dose coronary computed tomographic angiography*. *European Heart Journal*, 2011. **32**(21): p. 2625-2625.
  52. Beard, P., *Biomedical photoacoustic imaging*. *Interface focus*, 2011. **1**(4): p. 602-631.
  53. Rowland, K.J., et al., *Immediate alterations in intestinal oxygen saturation and blood flow after massive small bowel resection as measured by photoacoustic microscopy*. *Journal of pediatric surgery*, 2012. **47**(6): p. 1143-1149.
  54. S. Myerson, J.M.F., and S. Neubauer, *Cardiovascular Magnetic Resonance*. 1st ed ed2010: Oxford University Press.
  55. Stevens, G.R., N. Fida, and J. Sanz, *Computed tomography and cardiac magnetic resonance imaging in pulmonary hypertension*. *Progress in cardiovascular diseases*, 2012. **55**(2): p. 161-171.
  56. Yilmaz, A., et al., *Role of cardiovascular magnetic resonance imaging (CMR) in the diagnosis of acute and chronic myocarditis*. *Heart failure reviews*, 2012: p. 1-14.
  57. Mavrogeni, S., et al., *The diagnostic role of cardiac magnetic resonance imaging in detecting myocardial inflammation in systemic lupus erythematosus. Differentiation from viral myocarditis*. *Lupus*, 2013. **22**(1): p. 34-43.
  58. Raman, S.V., A. Aneja, and W.N. Jarjour, *CMR in inflammatory vasculitis*. *Journal of Cardiovascular Magnetic Resonance*, 2012. **14**(1): p. 82.
  59. Wu, K.C., *CMR of microvascular obstruction and hemorrhage in myocardial infarction*. *Journal of Cardiovascular Magnetic Resonance*, 2012. **14**(1): p. 68.
  60. Pelc, N.J., et al., *Phase contrast cine magnetic resonance imaging*. *Magnetic resonance quarterly*, 1991. **7**(4): p. 229-254.



61. Bellenger, N.G., et al., *Left ventricular quantification in heart failure by cardiovascular MR using prospective respiratory navigator gating: Comparison with breath-hold acquisition*. Journal of Magnetic Resonance Imaging, 2000. **11**(4): p. 411-417.
62. Schulte, B., Beyer, *MRT des Herzens und der Gefäße* 2005: Springer.
63. Lotz, J., et al., *Cardiovascular flow measurement with Phase-Contrast MR imaging: Basic facts and implementation I*. Radiographics, 2002. **22**(3): p. 651-671.
64. Srichai, M.B., et al., *Cardiovascular applications of phase-contrast MRI*. American Journal of Roentgenology, 2009. **192**(3): p. 662-675.
65. Moran, P.R., *A flow velocity zeugmatographic interlace for NMR imaging in humans*. Magnetic resonance imaging, 1982. **1**(4): p. 197-203.
66. Klipstein, R.H., et al., *Blood flow patterns in the human aorta studied by magnetic resonance*. British heart journal, 1987. **58**(4): p. 316-323.
67. Brenner, L.D., et al., *Quantification of left to right atrial shunts with velocity-encoded cine nuclear magnetic resonance imaging*. Journal of the American College of Cardiology, 1992. **20**(5): p. 1246-1250.
68. Chai, P. and R. Mohiaddin, *How we perform cardiovascular magnetic resonance flow assessment using phase-contrast velocity mapping*. Journal of Cardiovascular Magnetic Resonance, 2005. **7**(4): p. 705-716.
69. Nagel, E., et al., *Noninvasive determination of coronary blood flow velocity with cardiovascular magnetic resonance in patients after stent deployment*. Circulation, 2003. **107**(13): p. 1738-1743.
70. Brix, L., et al., *Journal of Cardiovascular Magnetic Resonance*. Journal of Cardiovascular Magnetic Resonance, 2009. **11**: p. 3.
71. Markl, M., et al., *Time-resolved three-dimensional phase-contrast MRI*. Journal of Magnetic Resonance Imaging, 2003. **17**(4): p. 499-506.
72. Baltes, C., et al., *Retrospective respiratory motion correction for navigated cine velocity mapping*. Journal of Cardiovascular Magnetic Resonance, 2004. **6**(4): p. 785-792.
73. Larson, A.C., et al., *Self-gated cardiac cine MRI*. Magnetic Resonance in Medicine, 2004. **51**(1): p. 93-102.
74. Petersson, S., et al., *Retrospectively gated intra-cardiac 4D flow CMR using spiral k-space trajectories*. Journal of Cardiovascular Magnetic Resonance, 2013. **15**(Suppl 1): p. O64.
75. Markl, M., et al., *Generalized reconstruction of phase contrast MRI: analysis and correction of the effect of gradient field distortions*. Magnetic Resonance in Medicine, 2003. **50**(4): p. 791-801.
76. Walker, P.G., et al., *Semiautomated method for noise reduction and background phase error correction in MR phase velocity data*. Journal of Magnetic Resonance Imaging, 1993. **3**(3): p. 521-530.
77. Meier, S., et al., *Towards Patient-Individual Blood Flow Simulations based on PC-MRI Measurements*.
78. Stalder, A., et al., *Quantitative 2D and 3D phase contrast MRI: optimized analysis of blood flow and vessel wall parameters*. Magnetic Resonance in Medicine, 2008. **60**(5): p. 1218-1231.
79. Ebbers, T., et al., *Noninvasive measurement of time-varying three-dimensional relative pressure fields within the human heart*. Journal of biomechanical engineering, 2002. **124**(3): p. 288-293.
80. Osinnski, J.N., et al., *Determination of wall shear stress in the aorta with the use of MR phase velocity mapping*. Journal of Magnetic Resonance Imaging, 1995. **5**(6): p. 640-647.
81. Oyre, S., et al., *Automatic accurate non-invasive quantitation of blood flow, cross-sectional vessel area, and wall shear stress by modelling of magnetic resonance velocity data*. European journal of vascular and endovascular surgery, 1998. **16**(6): p. 517-524.
82. Dyverfeldt, P., et al., *On MRI turbulence quantification*. Magnetic resonance imaging, 2009. **27**(7): p. 913-922.

83. Reiter, G., et al., *Magnetic resonance-derived 3-dimensional blood flow patterns in the main pulmonary artery as a marker of pulmonary hypertension and a measure of elevated mean pulmonary arterial pressure*. *Circulation: Cardiovascular Imaging*, 2008. **1**(1): p. 23-30.
84. Harloff, A., et al., *In vivo assessment of wall shear stress in the atherosclerotic aorta using flow-sensitive 4D MRI*. *Magnetic Resonance in Medicine*, 2010. **63**(6): p. 1529-1536.
85. Hoskins, P., *Accuracy of maximum velocity estimates made using Doppler ultrasound systems*. *British Journal of Radiology*, 1996. **69**(818): p. 172-177.
86. EVANS, A.J., et al., *Magnetic resonance imaging of blood flow with a phase subtraction technique: in vitro and in vivo validation*. *Investigative Radiology*, 1993. **28**(2): p. 109-115.
87. Johnson, K.M., et al., *Improved 3D phase contrast MRI with off-resonance corrected dual echo VIPR*. *Magnetic Resonance in Medicine*, 2008. **60**(6): p. 1329-1336.
88. Lum, D.P., et al., *Transstenotic Pressure Gradients: Measurement in Swine—Retrospectively ECG-gated 3D Phase-Contrast MR Angiography versus Endovascular Pressure-sensing Guidewires*. *Radiology*, 2007. **245**(3): p. 751-760.
89. Gutberlet, M., et al., *Arterial Switch Procedure for D-Transposition of the Great Arteries: Quantitative Midterm Evaluation of Hemodynamic Changes with Cine MR Imaging and Phase-Shift Velocity Mapping—Initial Experience*. *Radiology*, 2000. **214**(2): p. 467-475.
90. Bock, J., et al., *In vivo noninvasive 4D pressure difference mapping in the human aorta: phantom comparison and application in healthy volunteers and patients*. *Magnetic Resonance in Medicine*, 2011. **66**(4): p. 1079-1088.
91. Krittitan, S., et al., *A finite-element approach to the direct computation of relative cardiovascular pressure from time-resolved MR velocity data*. *Med Image Anal*, 2012. **16**(5): p. 1029-1037.
92. Meier, S., et al., *A fast and noise-robust method for computation of intravascular pressure difference maps from 4d PC-MRI data*, in *Statistical Atlases and Computational Models of the Heart. Imaging and Modelling Challenges 2013*, Springer. p. 215-224.
93. Meier, S., et al. *Non-invasive 4D blood flow and pressure quantification in central blood vessels via PC-MRI*. in *Computing in Cardiology, 2010*. 2010. IEEE.
94. Watanabe, H., S. Sugiura, and T. Hisada, *The looped heart does not save energy by maintaining the momentum of blood flowing in the ventricle*. *American Journal of Physiology-Heart and Circulatory Physiology*, 2008. **294**(5): p. H2191-H2196.
95. Kilner, P.J., *Letter to the editor: "Postulated functional advantages of a looped as opposed to a linearly arranged heart"*. *American Journal of Physiology-Heart and Circulatory Physiology*, 2010. **298**(2): p. H726-H726.
96. Yoshida, T., et al., *Lack of inertia force of late systolic aortic flow is a cause of left ventricular isolated diastolic dysfunction in patients with coronary artery disease*. *Journal of the American College of Cardiology*, 2006. **48**(5): p. 983-991.
97. Sugawara, M., et al., *Aortic blood momentum—the more the better for the ejecting heart in vivo?* *Cardiovasc Res*, 1997. **33**(2): p. 433-446.
98. Markl, M., P.J. Kilner, and T. Ebbers, *Comprehensive 4D velocity mapping of the heart and great vessels by cardiovascular magnetic resonance*. *J Cardiovasc Magn Reson*, 2011. **13**: p. 7.
99. Nordmeyer, S., et al., *Flow-sensitive four-dimensional cine magnetic resonance imaging for offline blood flow quantification in multiple vessels: a validation study*. *J Magn Reson Imaging*, 2010. **32**(3): p. 677-83.
100. [cited 2013; Available from: <http://www.mevis.fraunhofer.de/loesungen/cardiac-mri-inspection-of-the-heart-muscle.html>].
101. Kuehne, T., et al., *Influence of blood-pool contrast media on MR imaging and flow measurements in the presence of pulmonary arterial stents in swine*. *Radiology*, 2002. **223**(2): p. 439-45.
102. Hennemuth, A., et al. *Fast interactive exploration of 4D MRI flow data*. in *Medical Imaging 2011: Visualization, Image-Guided Procedures, and Modeling*. 2011.
103. Meier, S., et al. *Non-invasive 4D blood flow and pressure quantification in central blood vessels via PC-MRI in Computing in Cardiology*. 2010.

104. Meier, S., et al. *A Fast and Noise-Robust Method for Computation of Intravascular Pressure Difference Maps from 4D PC-MRI Data*. in *Statistical Atlases and Computational Models of the Heart. Imaging and Modelling Challenges*. 2013.
105. Mills, C.J., et al., *Pressure-flow relationships and vascular impedance in man*. Cardiovasc Res, 1970. **4**(4): p. 405-17.
106. Ou, P., et al., *Increased central aortic stiffness and left ventricular mass in normotensive young subjects after successful coarctation repair*. Am Heart J, 2008. **155**(1): p. 187-93.
107. Brown, H. and R. Prescott, *Applied Mixed Models in Medicine*, ed. L. John Wiley & Sons 1999, Chichester, New York, Weinheim, Brisbane, Singapore, Toronto.
108. Frydrychowicz, A., et al., *Three-dimensional analysis of segmental wall shear stress in the aorta by flow-sensitive four-dimensional-MRI*. J Magn Reson Imaging, 2009. **30**(1): p. 77-84.
109. Saouti, N., et al., *Aortic function quantified: the heart's essential cushion*. J Appl Physiol, 2012. **113**(8): p. 1285-91.
110. Nasiraei-Moghaddam, A., et al., *Factors affecting the accuracy of pressure measurements in vascular stenoses from phase-contrast MRI*. Magn Reson Med, 2004. **52**(2): p. 300-9.
111. Bock, J., et al., *In vivo noninvasive 4D pressure difference mapping in the human aorta: phantom comparison and application in healthy volunteers and patients*. Magn Reson Med, 2011. **66**(4): p. 1079-88.
112. Itu, L., et al., *Non-Invasive Hemodynamic Assessment of Aortic Coarctation: Validation with In Vivo Measurements*. Annals of Biomedical Engineering. **41**(4): p. 669-681.
113. Ebbers, T. and G. Farneback, *Improving computation of cardiovascular relative pressure fields from velocity MRI*. J Magn Reson Imaging, 2009. **30**(1): p. 54-61.
114. Krittian, S.B., et al., *A finite-element approach to the direct computation of relative cardiovascular pressure from time-resolved MR velocity data*. Med Image Anal, 2012. **16**(5): p. 1029-37.
115. Beerbaum, P., et al., *Cardiac function by MRI in congenital heart disease: impact of consensus training on interinstitutional variance*. J Magn Reson Imaging, 2009. **30**(5): p. 956-66.
116. Helbing, W. *Assessment of tricuspid valve function with cardiovascular magnetic resonance*. in *ESC CONGRESS 2009*. 2009. Barcelona.
117. Quail, M.A., et al., *Use of cardiovascular magnetic resonance imaging for TAVR assessment in patients with bioprosthetic aortic valves: comparison with computed tomography*. European Journal of Radiology, 2012.
118. *International Journal of Cardiology*. [cited 2013; Available from: <http://www.journals.elsevier.com/international-journal-of-cardiology/>].